1971

A study of early-late type S0-PCM signal bit synchronizers

Kuang-Cheng Hu

Department:

A STUDY OF EARLY-LATE GATE TYPE SØ-PCM SIGNAL BIT SYNCHRONIZERS

BY

KUANG-CHENG HU, 1942-

A THESIS

Presented to the Faculty of the Graduate School of the

UNIVERSITY OF MISSOURI-ROLLA

In Partial Fulfillment of the Requirements for the Degree

MASTER OF SCIENCE IN ELECTRICAL ENGINEERING

1971

Approved by

_____ (Advisor) _____

_____

ABSTRACT

The steady-state phase noise performances of an absolute value type and a squaring loop type of early-late gate SØ-PCM signal bit synchronizers are developed using the Fokker-Planck method. The results are compared on the basis of the performance of two configurations with equal loop bandwidth at each input signal-to-noise ratio R_s. The probabilities of bit-detection error of the two configurations are compared. These comparisons are made as a function of R_s. The absolute value type of early-late gate SØ-PCM signal bit synchronizater yields better performance than that of the squaring loop type of early-late gate SØ-PCM signal bit synchronizer at every value of R_s.

ACKNOWLEDGEMENT

The author expresses his appreciation to Dr. Thomas L. Noack for the suggestion of this thesis topic and for the many helpful discussions concerning this work.

TABLE OF CONTENTS

Page

APPENDICES

LIST OF ILLUSTRATIONS

Figures

I. INTRODUCTION

A bit synchronizer is a device employed to derive the timing information for the associated bit detection element to reconstruct the transmitted digital data. Several kinds of data-derived bit synchronization systems are available in the literature[2,3,6,8]. Already receiving wide attention is the early-late-gate-integration type of bit synchronizer. A general form of the early-late-gate-integration type of bit synchronizer is shown in Figure 1.

As shown in Figure 1, the early-late-gate-integration type of bit synchronizer consists of a bit synchronization portion and a bit detection portion. The bit synchronization portion is essentially a phase-locked loop circuit which consists of a phase detector, a loop filter and a voltage-controlled oscillator (VCO). The bit detection portion consists of a detection device and decision logic. For the phase detector there are various possible circuit topologies available[1], as shown in Figure 2. Of these, two circuits are studied in this paper; namely, the absolute value type (Figure 2c) and squaring loop type (Figure 2b). In this study, the bit synchronizers considered will be called the absolute value type of early-late-gate-integration type of bit synchronizer (AVBS) and squaring loop type of early-late-gate-integration type of bit synchronizer (SLBS).

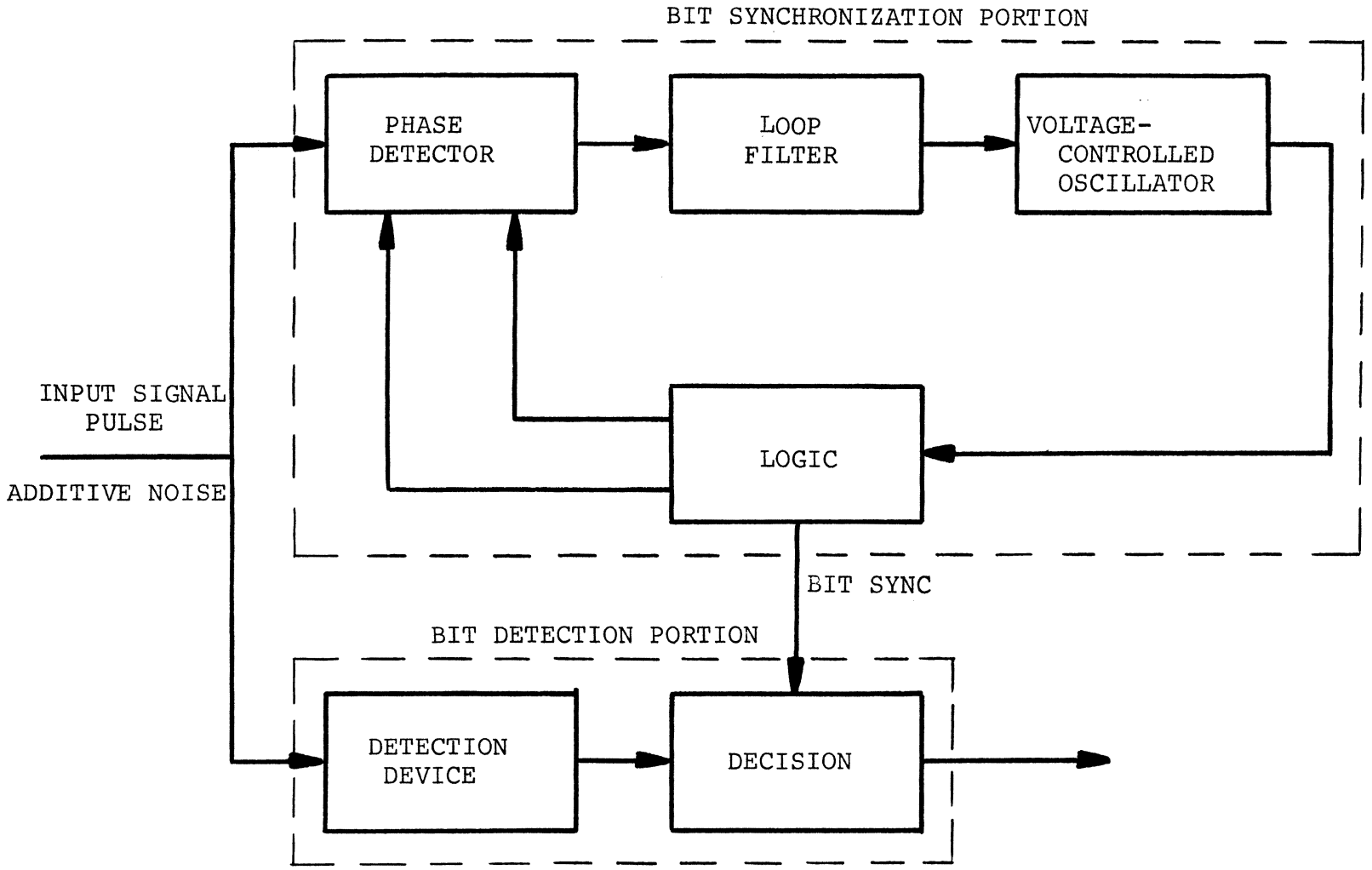

Figure 1. General Model of Early-Late-Gate-Integration Type of Bit Synchronizer.

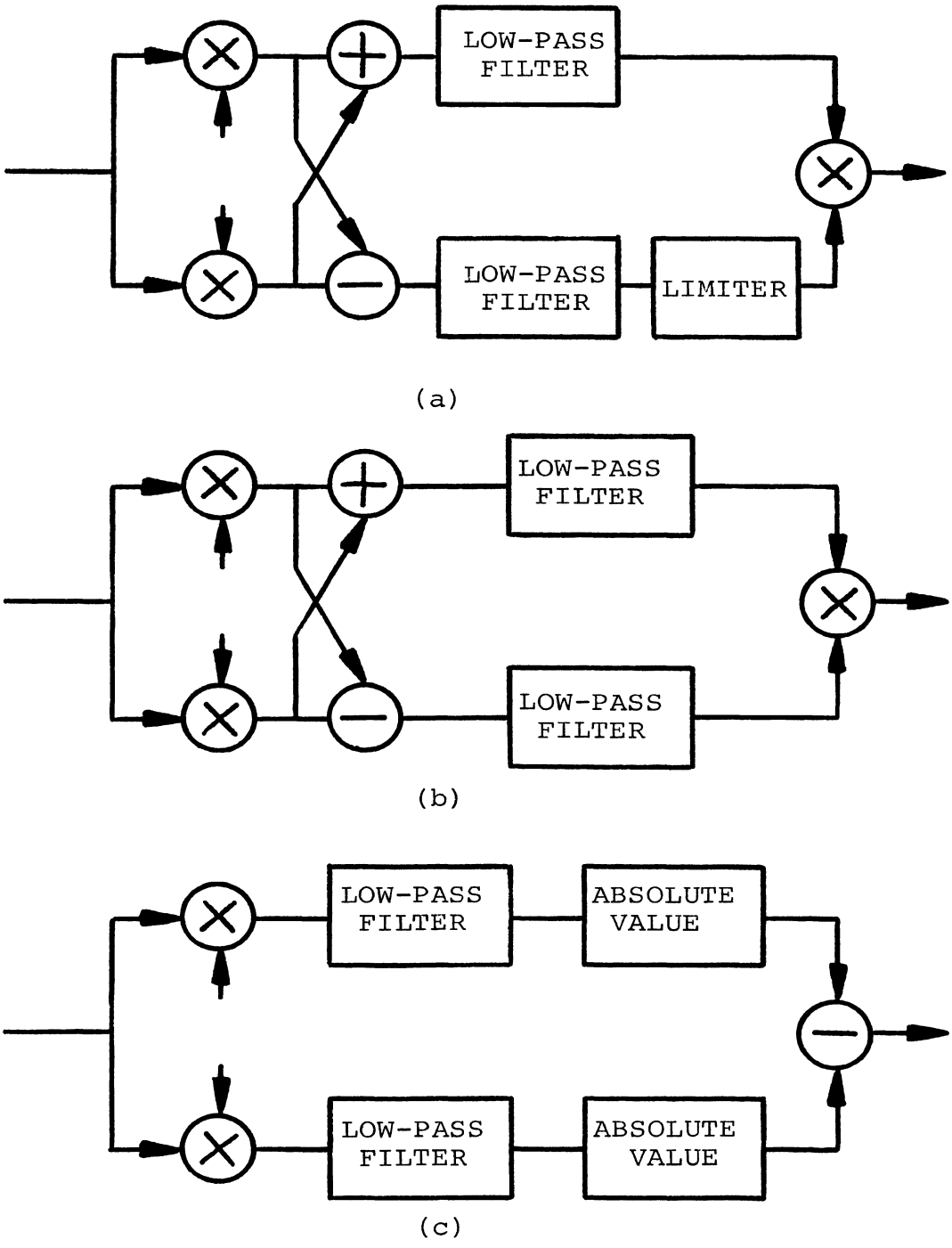

Figure 2. Bit Synchronizer Phase Detector Topologies: (a) Limiter Approximation; (b) Analog Multiplier; (c) Absolute Value.

The input signal considered here is of a split-phase pulse-code modulation (SØ-PCM) type. This type of waveform is analyzed because of its desirable bandwidth requirements and transition density characteristics. The detection of a SØ-PCM signal in the presence of noise requires precise timing synchronization for use in the bit detection circuitry. Due to the unique characteristic of the transition in the mid-bit of the SØ-PCM signal, mid-bit detection is employed and the symmetrical gate length of the early-gate and late-gate is used. Because of the symmetry of the two gates, DC drifts due to temperature will tend to cancel in the subtractor. Two modes of gate length are investigated; one is one-fourth of a bit interval and the other is one-eighth of a bit interval.

The bit synchronization portion constructs an error signal from the transition in the mid-bit of the received SØ-PCM signal; a phase-locked tracking loop then provides a timing estimate for use in the bit detection elements. This tracking process defines the temporal position of a bit within the received serial SØ-PCM signal. By specifying the statistics of the error signal, the loop S-curve $g(\lambda)$ and the spectrum of additive noise $S(\omega,\lambda)$, an equivalent phase-locked loop can be formed. By this equivalent phase-locked loop, the mean square phase noise σ_λ^2 of the bit synchronizer can be obtained via Fokker-Planck techniques.

The resulting mean square phase noise σ_{λ}^{2} will be compared between the two types of bit synchronizer under investigation.

The bit detection portion extracts the timing information from the bit synchronization portion. The received input SØ-PCM signal and additive noise are passed through a split-phase to non-return-to-zero (SØ-NRZ) converter and then a matched filter. The output of the matched filter is compared to a threshold within the decision device to give outputs of the reconstructed digital data. The probabilities of error for the two bit synchronizers are calculated under various signal-to-noise ratio (SNR). Finally, the comparison of the two bit synchronizers is made.

II. REVIEW OF THE LITERATURE

Extensive research has been conducted in the field of data-derived bit synchronization telemetry communication systems. The analysis of the early-late-gate-integration type of bit synchronizer has received wide attention.

The more recent studies of data-derived bit synchronization system include the work of Wintz and Luecke[2]. An optimum synchronizer and a subsequent sub-optimum synchronizer are developed. Their suboptimal synchronization realization is formed by a cascade of a low-pass filter, a square-law nonlinearity, and a bandpass filter centered at the bit rate. A significant result of this study indicated that the square pulse which is commonly used in signaling does not perform as well as either the half-sine or raised-cosine pulses. Using these modified pulse shapes, near optimum performance can be achieved by the sub-optimum system.

Digital-data tracking loop performance has been analyzed theoretically by several authors. Lindsey and Tausworthe[3] analyze the steady-state phase-noise performance of this loop. An error signal, formed by the product of the in-phase and mid-phase channels, is used to drive the loop to synchronize. The loop S-curve $g(\lambda)$ and the spectrum of additive noise about the origin $S(0,0)$ are found as functions of the normalized phase error within the tracking loop. These curves permit use of an equivalent data-

transition tracking loop model. Lindsey and Tausworthe determine these nonlinearities analytically, and then apply the Fokker-Planck equation to find the mean square phase noise in the tracking loop as a function of input signal-to-noise ratio. Lindsey and Tausworthe also mention that an improvement in mean square phase noise can be accomplished by integrating in the mid-phase channel only over a portion of the symbol time. Simon[4] analyzes the digital-data tracking loop performance without the assumptions made by Lindsey and Tausworthe[3], thus yielding a more exact result. The performances of the full integration length and one-half integration length in mid-phase channel over the symbol time is investigated. The two solutions for mean square phase noise about any lock point as a function of signal-to-noise ratio R_s are compared. As the symbol rate increases and bandwidth decreases at fixed R_s the differences between the two answers becomes increasingly smaller. However, for the low-data-rate communication, the discrepancy between the results might be significant. A digital-data tracking-loop of bit synchronizer is mechanized by Lindsey and Anderson[5]. The tracking loop is developed to have an adaptive loop bandwidth dependent upon whether it is in acquisition or tracking mode.

Performance of the squaring loop type of early-late-gate-integration bit synchronizer has been investigated by Stiffler[6] and Layland[7]. Stiffler investigates the

subsequent effects upon performance with the signal shape and the type of feedback signal used within the loop varied. Both raised-cosine and rectangular pulses as the input signal shapes are tested, and the loop feedback signals are either sampling pulses or sinusoids. By using the phase error variance as a performance criterion, Stiffler concludes that the overall synchronizer performance is dependent upon both parameter variations and the specific combination of elements used. From the probabilistic transitions of the data signal derived, Layland[7] finds out that the error signal from the squaring loop depends only upon the relative positions of the transition time and the estimation time. It does not depend upon the sign of the data transition. Using the first-order linear bit tracking loop, the mean-square phase noise is derived as a function of input signal-to-noise ratio. Employing the effective signal-to-noise ratio at the output of the data correlator, Layland finds that if this effective signal-to-noise ratio is only slightly degraded by the timing jitter, the increase in error probability due to timing jitter will also be slight.

The steady-state phase noise performance of an absolute value type of an early-late gate bit synchronizer was investigated by Simon[8]. The loop S-curve and spectral density of the equivalent noise versus signal-to-noise ratio characteristics are specified. Using the equivalent phase-locked loop model, the mean square phase noise is

computed as a function of input signal-to-noise ratio for various values of bandwidth-symbol time product by applying the Fokker-Planck equation. The results are compared with the performance of digital-data transition tracking type and squaring loop type of early-late gate bit synchronizers on the basis of either 1) equal equivalent SNR in the loop bandwidth in the linear region, or 2) equal loop bandwidth at each input signal-to-noise ratio R_s. These comparisons are made as a function of R_s. Simon concludes that, in both cases, the absolute value type of early-late gate bit synchronizer yields the best performance in the sense of minimum phase noise at every value of R_s.

The performance of a noncoherent frequency-shift-keyed system utilizing split-phase waveforms under conditions of noisy synchronizing signal is investigated by Glenn and Lieberman[9]. The split-phase waveform is converted to return-to-zero format in order to extract synchronization information. The root-mean-squared VCO phase jitter is derived as a function of SNR. In order to have optimum detection, the split-phase waveform is converted to non-return-to-zero form so as to be match filtered. The probability of error is calculated as a function of SNR and timing error.

McBride and Sage[10] develop an optimum maximum-a-posteriori(MAP) estimation algorithm to provide timing estimation for data-derived digital bit synchronization systems. Use of the Karhunen-Loeve expansion permits analytical investigation of the synchronization problem, finding the MAP estimate of phase error θ. Several sub-optimal synchronizers are proposed.

III. SYSTEM DESCRIPTION

A. Bit Synchronization Portion

Functional diagrams of the absolute value type bit synchronizer (AVBS) and squaring loop type bit synchronizer (SLBS) are given in Figure 3 and Figure 4, respectively. The operation of these loops is given as follows:

The input y(t) is passed through two parallel channels which are triggered by a timing generator according to an error signal formed from the difference of the channel outputs. Furthermore, the two channels are held at a fixed phase relationship with one another by the timing generator. These two channels can be referred to as the early channel and the late channel by the use of early integral and late integral, respectively. Each integral is taken over fraction of full bit interval, Δ, which will be one-fourth and one-eighth of full bit interval. The two integrals are nonoverlapping symmetrical with the early integral starting ΔT early, and the late integral ΔT late. In fact, the output of the late channel J_k should be delayed by an amount τ before subtracting the appropriate I_k. Actually, this delay has negligible effect on the noise analysis of the loop operation when $W_L T >> 1$, where W_L is the two-sided loop bandwidth[11]. In this study the delay factor for the late channel is neglected. Synchronization in the loop is described in the following.

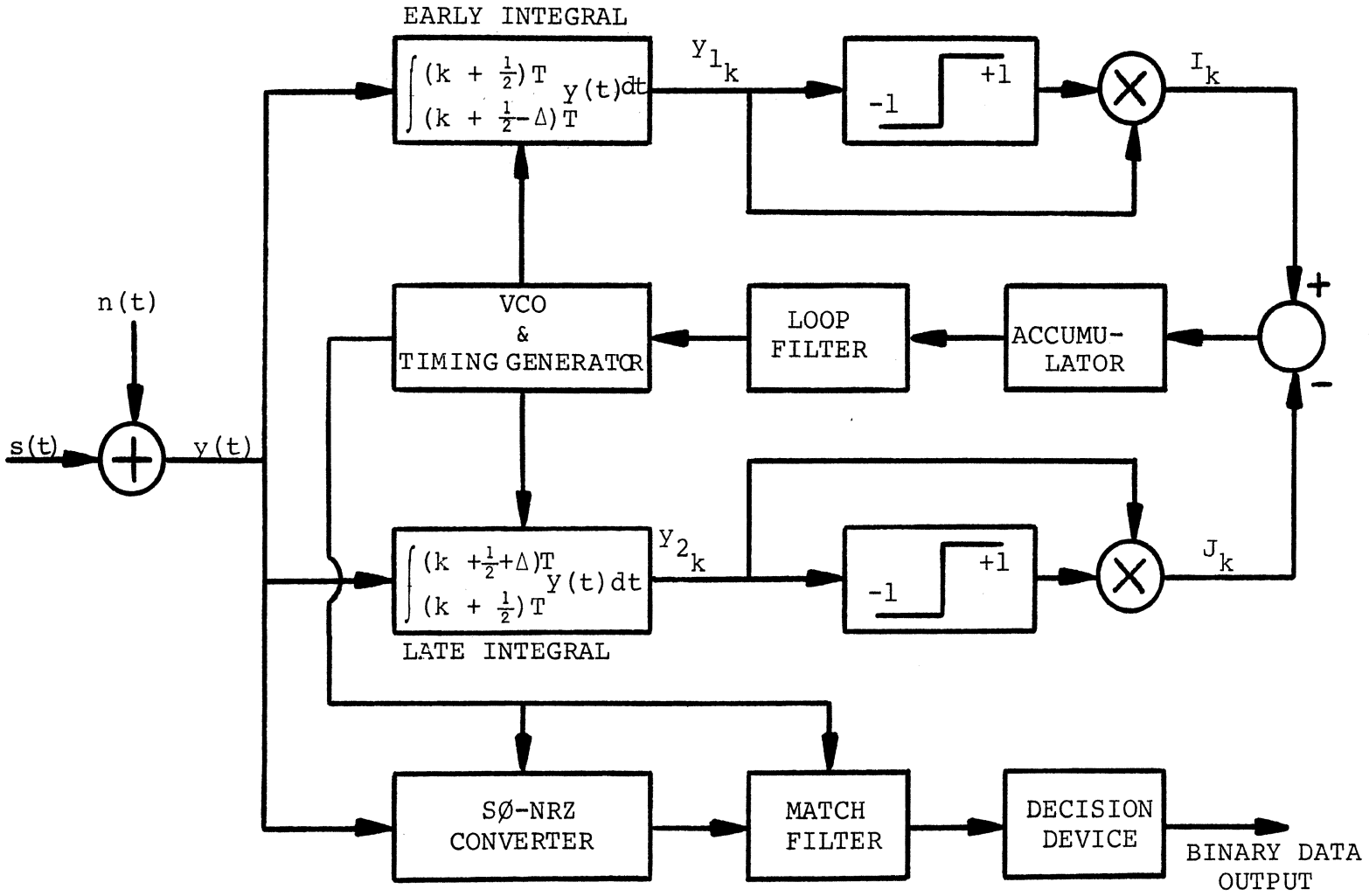

Figure 3. Functional Absolute Value Type Bit Synchronizer.

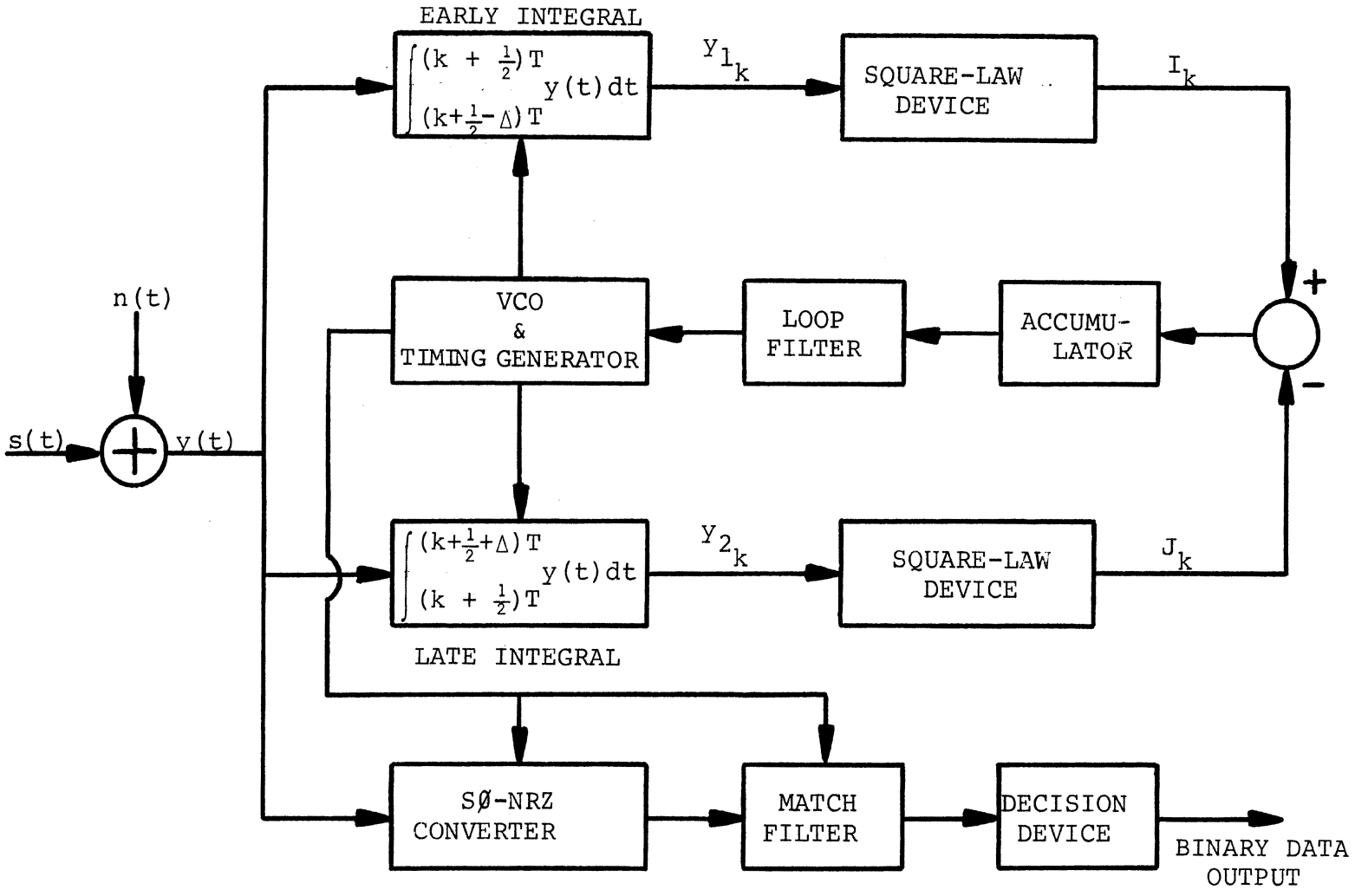

Figure 4. Functional Squaring Loop Type Bit Synchronizer.

The input SØ-PCM signal is a random pulse train, representing the data symbol, i.e.,

$$s(t) = \sum_n [d_n p(t - nT - \varepsilon(t)) - d_n p(t - (n + \tfrac{1}{2})T - \varepsilon(t))] \quad (1)$$

where

$$p(t) = \begin{cases} 1 \text{ for } 0 \leq t \leq T/2, \\ 0 \text{ for all other } t, \end{cases}$$

T = the symbol period,

d_n = the symbol amplitude, which takes on the values $\pm A$ with equal probability,

and $\varepsilon(t)$ = the random epoch to be estimated.

The input additive noise process $n(t)$ is assumed to be white Gaussian with a two-sided spectral density $N_o/2$. The early integral filter and the late integral filter are, in principle, matched filters to the input. The outputs of the early integral and the late integral are sampled periodically every T seconds. As for the AVBS case, the outputs of the early integral y_{1_k} and the late integral y_{2_k} are passed through hard limiters and then multiplied by the y_{1_k} and y_{2_k}, respectively. The outputs of the two channels I_k and J_k are thus obtained. As for the SLBS case, the outputs of the early integral y_{1_k} and the late integral y_{2_k} are passed through square-law devices to give the channel outputs I_k and J_k, respectively. An error signal

e_k is obtained by $I_k - J_k$. The error signal e_k is accumulated for an interval NT and then digitally filtered by the loop filter with the resulting output being used to control the instantaneous frequency (phase) of the timing generator. An estimate, $\hat{\varepsilon}(t)$, of the input random epoch is thus formed and the phase difference $\lambda - (\varepsilon - \hat{\varepsilon})/T$ is used to drive the loop. For the AVBS case, examples of the appropriate waveforms in the absence of noise in the early channel and the late channel for a typical input sequence are illustrated by Figure 5 and Figure 6. Figure 5 is for the case of perfect synchronization, i.e., $\lambda = 0$, and Figure 6 is for the case of synchronization error, $\lambda \neq 0$.

B. Bit Detection Portion

The bit detection configuration is shown in Figure 3 and Figure 4 for the AVBS and SLBS, respectively. For the two types of bit synchronizer under investigation, the bit detection segments are the same.

The input y(t) is first converted from a split-phase waveform to a non-return-to-zero waveform. This conversion is made possible by using the timing information from the bit synchronization portion to form the switching pulses. The non-return-to-zero waveforms are then matched filtered and sampled every T seconds. The sampling pulses are taken from the bit synchronization portion. The sampled outputs are passed through the decision device to give the

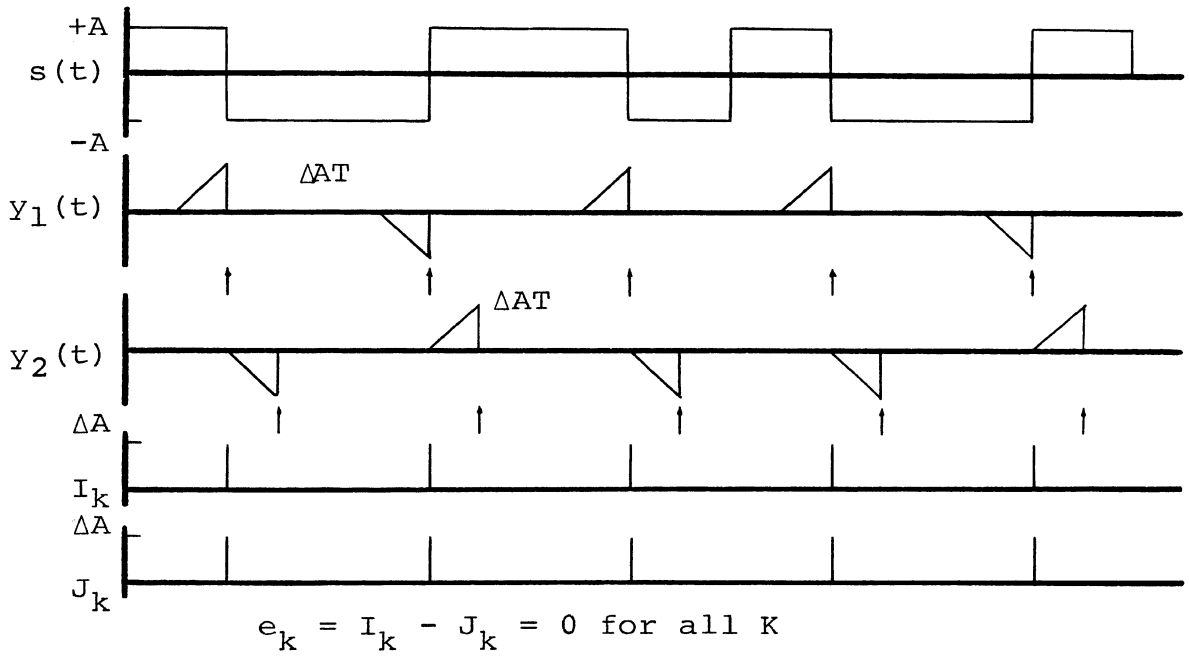

Figure 5. Loop Waveforms (Ideal Integrate and Dump) Perfect Synchronization, for AVBS Configuration.

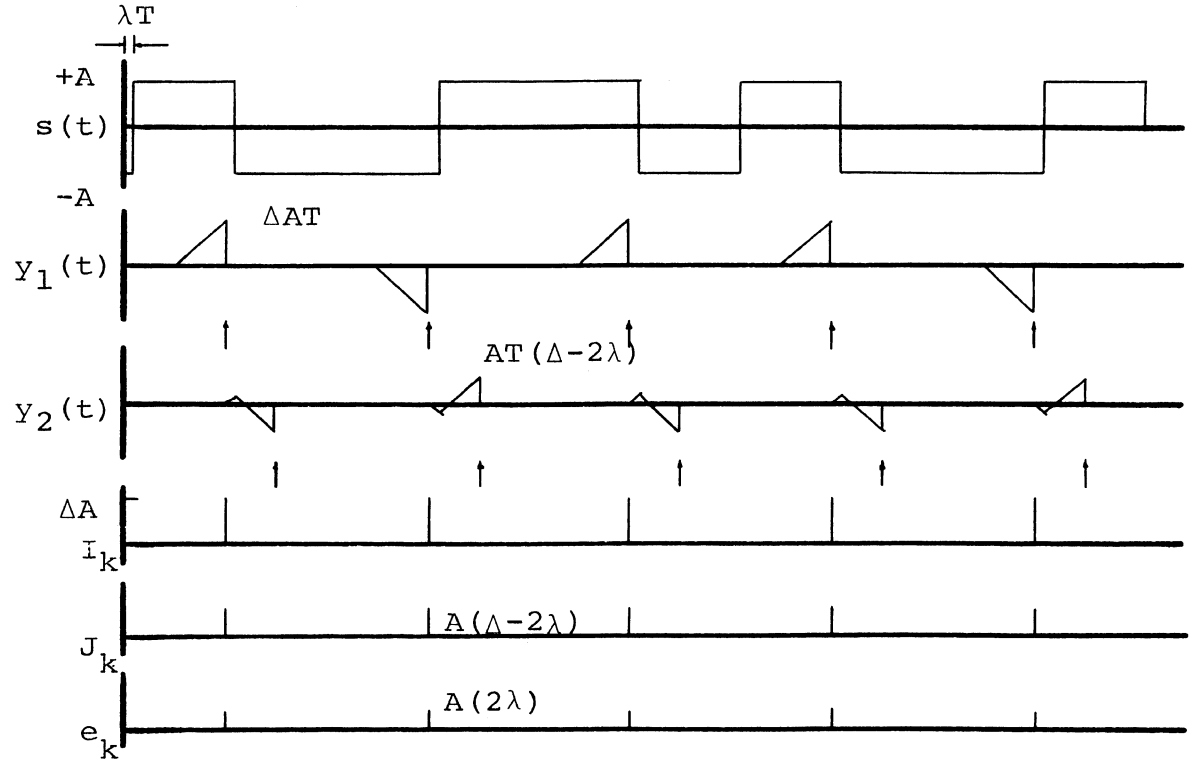

Figure 6. Loop Waveforms (Ideal Integrate and Dump) Imperfect Synchronization, for AVBS Configuration.

binary outputs. Examples of the appropriate waveforms in the absence of noise at various points in the bit detector for a typical input sequence are illustrated by Figure 7. Figure 7a is for the case of perfect synchronization, i.e., $\lambda = 0$, and Figure 7b is for the case $\lambda \neq 0$.

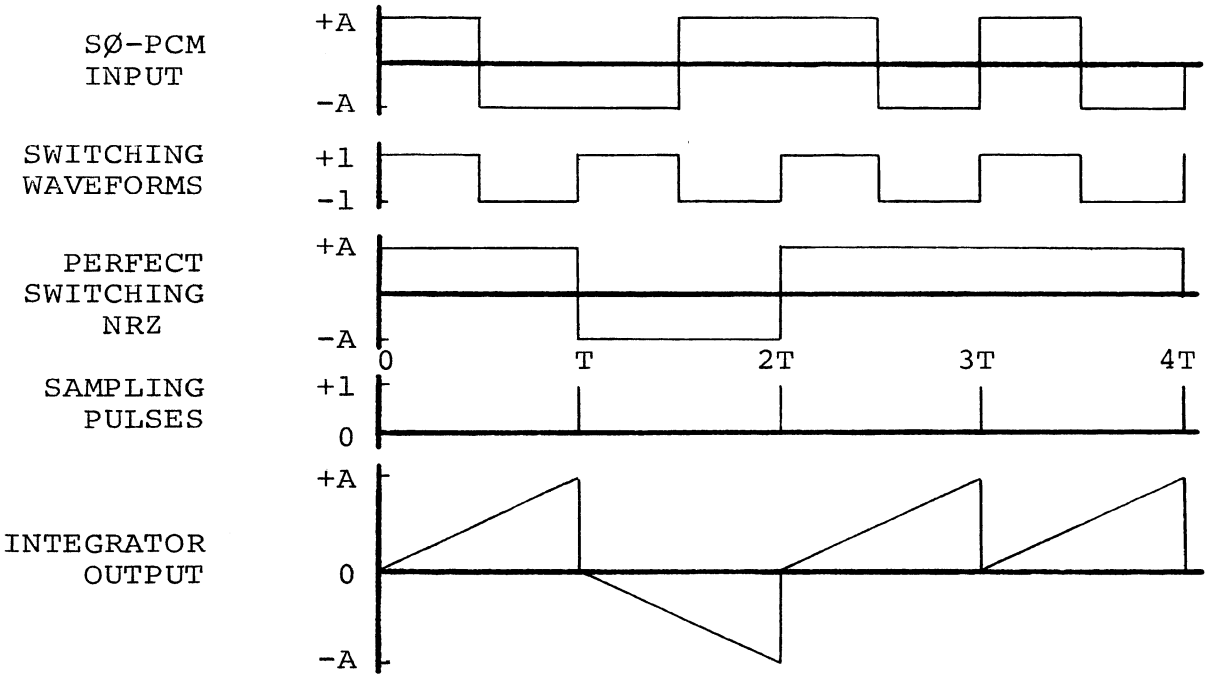

Figure 7a. Effect of Perfect Synchronization on NRZ Waveforms.

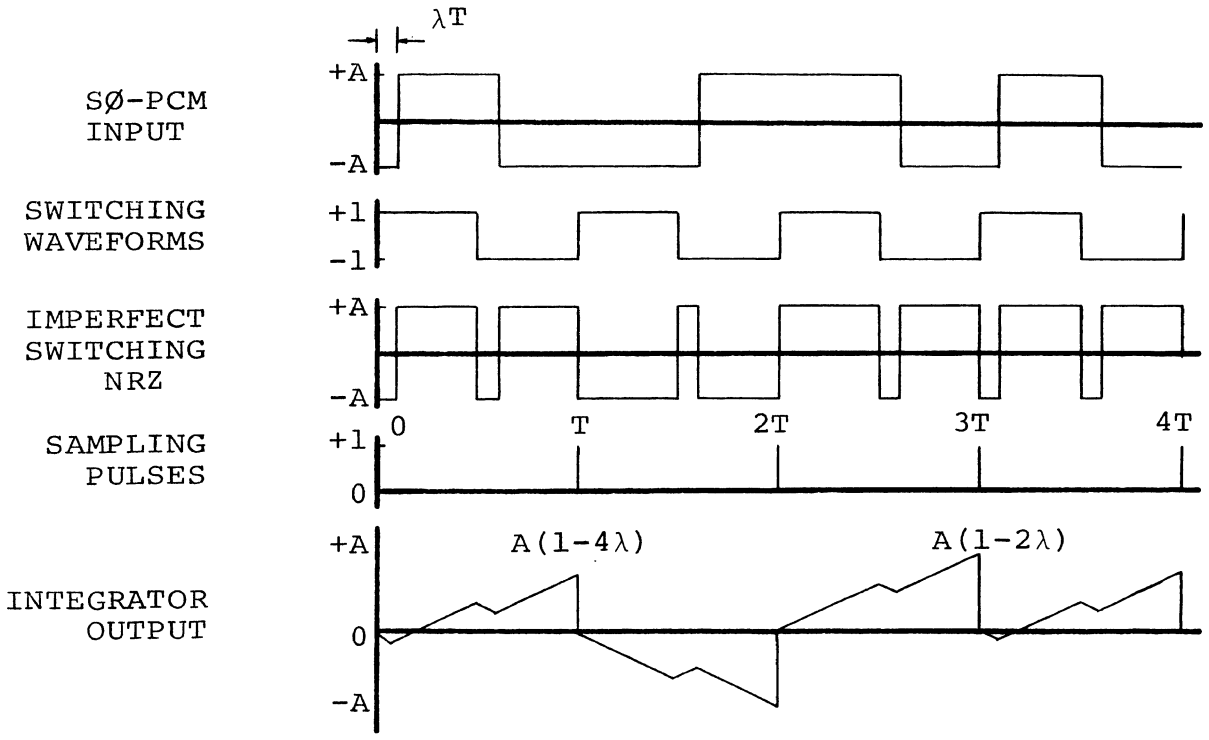

Figure 7b. Effect of Imperfect Synchronization on NZR Waveforms.

IV. SYSTEM ANALYSIS

A. Loop S-curve $g(\lambda)$ and Spectrum of Additive Noise $S(\omega,\lambda)$

The symbol tracker can be represented by an equivalent phase-locked loop whose steady-state performance can be found by applying the Fokker-Planck equation. The assumptions under which such a representation is valid are given by Simon[8] and will be given below.

Developing the above-mentioned equivalent phase-locked loop relies on finding 1) the average loop S-curve $g(\lambda)$ as a function of the normalized phase error $\lambda = (\varepsilon - \hat{\varepsilon})/T$, and 2) the two-sided spectral density about the origin, $S(\omega,\lambda)$, of the equivalent additive noise, $n_\lambda(t)$ at the output of the loop nonlinearity $g(\lambda)$. Once these quantities are determined the equivalent phase-locked loop may be represented as shown in Figure 8.

The approach taken in finding $g(\lambda)$ and $S(\omega,\lambda)$ follows that of Lindsey and Tausworthe[3]. The assumptions that must be imposed on the system are as follows:

(1) The perturbations of the actual transition times about their nominal values are essentially constant over a large number of symbol intervals.

(2) The estimates of these perturbations are essentially constant over a large number of symbol intervals. This will be true if the response of the equivalent phase-locked loop is very slow with respect to a symbol interval, i.e., $W_L T << 1$.

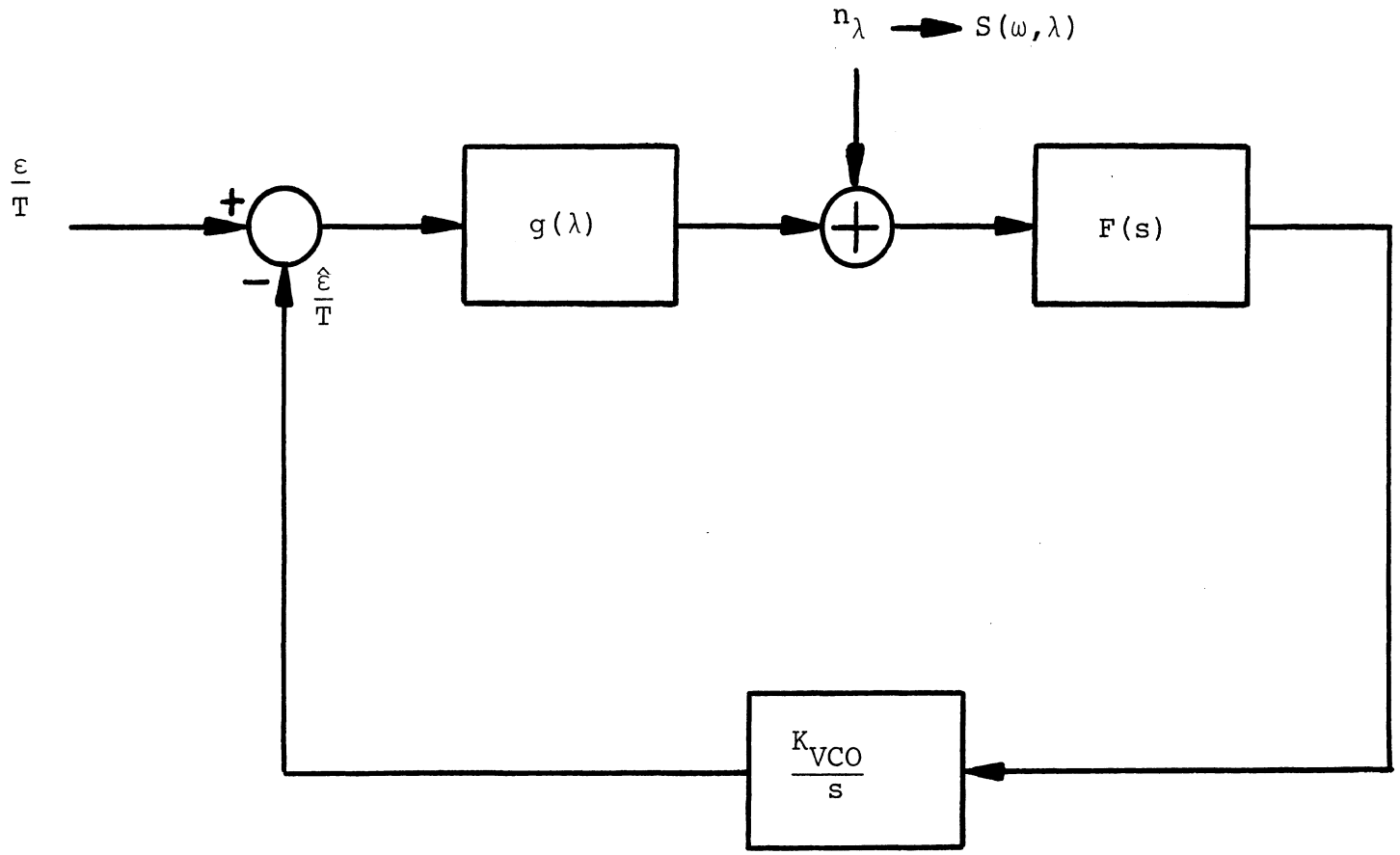

Figure 8. Equivalent Phase-Locked Loop for AVBS and SLBS Configurations

It follows from (1) and (2) that the loop can be analyzed as a continuous loop, and that the statistics of the random variable e_k can be determined assuming $\lambda = (\varepsilon - \hat{\varepsilon})/T$ to be fixed. In effect, then this is to consider many records of the discrete random variable e_k at fixed λ and call the average value of this ensemble $g(\lambda)$, and its spectrum $S(\omega,\lambda)$. The actual spectrum $S(\omega)$ of the additive noise is then obtained by averaging $S(\omega,\lambda)$ over the distribution of , $P(\lambda)$, which is to be found; i.e.,

$$S(\omega) = \int_{-\Delta}^{\Delta} S(\omega,\lambda)P(\lambda)\, d\lambda \tag{2}$$

With reference to Figure 3 and Figure 4, the preceding statements can be expressed mathematically as follows:

$$y_1(kT) = y_{1_k} = c_k + \nu_k \tag{3}$$

where

$$c_k = \int_{(k + \frac{1}{2} - \Delta)T}^{(k + \frac{1}{2})T} s(t)\, dt,$$

$$\nu_k = \int_{(k + \frac{1}{2} - \Delta)T}^{(k + \frac{1}{2})T} n(t)\, dt.$$

$$y_2((k + \tfrac{1}{2})T) = y_{2_k} = b_k + \mu_k \tag{4}$$

where

$$b_k = \int_{(k+\frac{1}{2})T}^{(k+\frac{1}{2}+\Delta)T} s(t)\,dt\ ,$$

$$\mu_k = \int_{(k+\frac{1}{2})T}^{(k+\frac{1}{2}+\Delta)T} n(t)\,dt\ .$$

In the above, Δ is the integration window length, having a length of 1/4 and 1/8 of a bit interval.

Since the early integral and the late integral are symmetrically nonoverlapped, ν_k and μ_k are statistically independent Gaussian random variables, each with zero mean and variance,

$$\sigma^2 = \sigma_\nu^2 = \sigma_\mu^2 = N_o\Delta T/2 \tag{5}$$

The error signal e_k can be found as

$$e_k = I_k - J_k \tag{6}$$

The loop S-curve $g(\lambda)$ is defined as

$$g(\lambda) = E_{n,s}\{e_k|\lambda\} \tag{7}$$

where $E_{n,s}$ represents the conditional expectation of λ both with respect to the noise and signal (symbol sequence).

The spectrum of the additive noise, n_λ, $S(\omega,\lambda)$ is defined by

$$S(\omega,\lambda) = \mathcal{F}\{E_{n,s}[\{e_k - E_{n,s}(e_k|\lambda)|\lambda\}\cdot\{e_{k+m} - E_{n,s}(e_{k+m}|\lambda)|\lambda\}]\}$$

$$= \mathcal{F}\{R(m,\lambda)\} \text{ if the error signal process is stationary} \tag{8}$$

The symbol F denotes the discrete Fourier transform, i.e.,

$$S(\omega,\lambda) = \sum_{m=-\infty}^{\infty} R(m,\lambda)\cos mT \tag{9}$$

Equation (8) can be rewritten as

$$S(\omega,\lambda) = F\{E_{n,s}(e_k e_{k+m}|\lambda) - g^2(\lambda)\} \tag{10}$$

With the assumptions and definitions made above the evaluation of $g(\lambda)$ and $S(\omega,\lambda)$ for the two types of bit synchronizer under investigation can be made as shown below.

(1) Absolute Value Type Bit Synchronizer

With reference to Figure 3, the error signal e_k is

$$e_k = (c_k + \nu_k)\ \mathrm{sgn}(c_k + \nu_k) - (b_k + \mu_k)\ \mathrm{sgn}(b_k + \mu_k) \tag{11}$$

The evaluation of $g(\lambda)$ is done in Appendix A, with the result

$$g_n(\lambda) = \frac{g(\lambda)}{2AT} = 1/2\{\Delta\,\mathrm{erf}(\Delta R_s)^{\frac{1}{2}} - (\Delta - 2\lambda)\,\mathrm{erf}[(\Delta - 2\lambda) \cdot (\frac{R_s}{\Delta})^{\frac{1}{2}}] + (\frac{\Delta}{\pi R_s})^{\frac{1}{2}}[\exp(-\Delta R_s) - \exp(-\frac{(\Delta - 2\lambda)^2 R_s}{\Delta})]\},$$

$$\lambda \leq \Delta. \tag{12}$$

where

$$R_s = A^2 T/N_o.$$

It can also be shown that $g(\lambda)$ is an odd function of λ. Figure 9 and Figure 11 illustrate the normalized nonlinearity $g_n(\lambda)$, defined above, as a function of R_s for $\Delta = 1/4$

and $\Delta = 1/8$ cases, respectively. The limiting curve ($R_s \to \infty$) is also indicated by dashed lines.

The computation of $S(\omega,\lambda)$ is done in Appendix B. Since $R(m,\lambda)$ has nonzero value only at $m = 0$, the spectrum consists of a constant component only. $S(\omega,\lambda)$ can be represented by $S(0,\lambda)$. The result is

$$\frac{S(0,\lambda)}{N_o \Delta T} = h(\lambda) \tag{13}$$

where

$$h(\lambda) = 1 + \Delta R_s\{1 - [\mathrm{erf}(\Delta R_s)^{\frac{1}{2}}]^2\} + \frac{(\Delta - 2\lambda)^2 R_s}{\Delta}\{1$$

$$- [\mathrm{erf}((\Delta - 2\lambda)\cdot(\frac{R_s}{\Delta})^{\frac{1}{2}})]^2\} - \frac{1}{\pi}\{[\exp(-\Delta R_s)]^2$$

$$+ [\exp(-\frac{(\Delta - 2\lambda)^2 R_s}{\Delta})]^2\} - (\frac{4R_s}{\pi\Delta})^{\frac{1}{2}}\{\Delta\,\mathrm{erf}(\Delta R_s)^{\frac{1}{2}} \cdot$$

$$\exp(-\Delta R_s) + (\Delta - 2\lambda)\,\mathrm{erf}[(\Delta - 2\lambda)(\frac{R_s}{\Delta})^{\frac{1}{2}}] \cdot$$

$$\exp(-\frac{(\Delta - 2\lambda)^2 R_s}{\Delta})\}\ , \quad \lambda \leq \Delta. \tag{14}$$

Figure 10 and Figure 12 illustrate the spectrum $S(0,\lambda)$ versus normalized phase error for various values of R_s for $\Delta = 1/4$ and $\Delta = 1/8$ cases, respectively

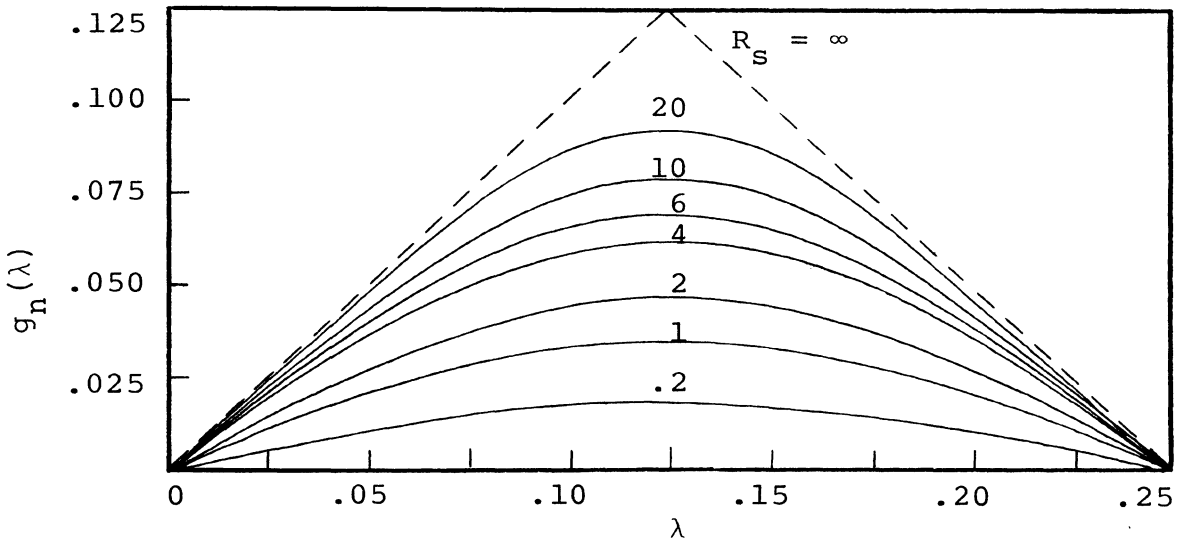

Figure 9. Loop Nonlinearity Versus Normalized Phase Error $\Delta = 1/4$, for AVBS Configuration.

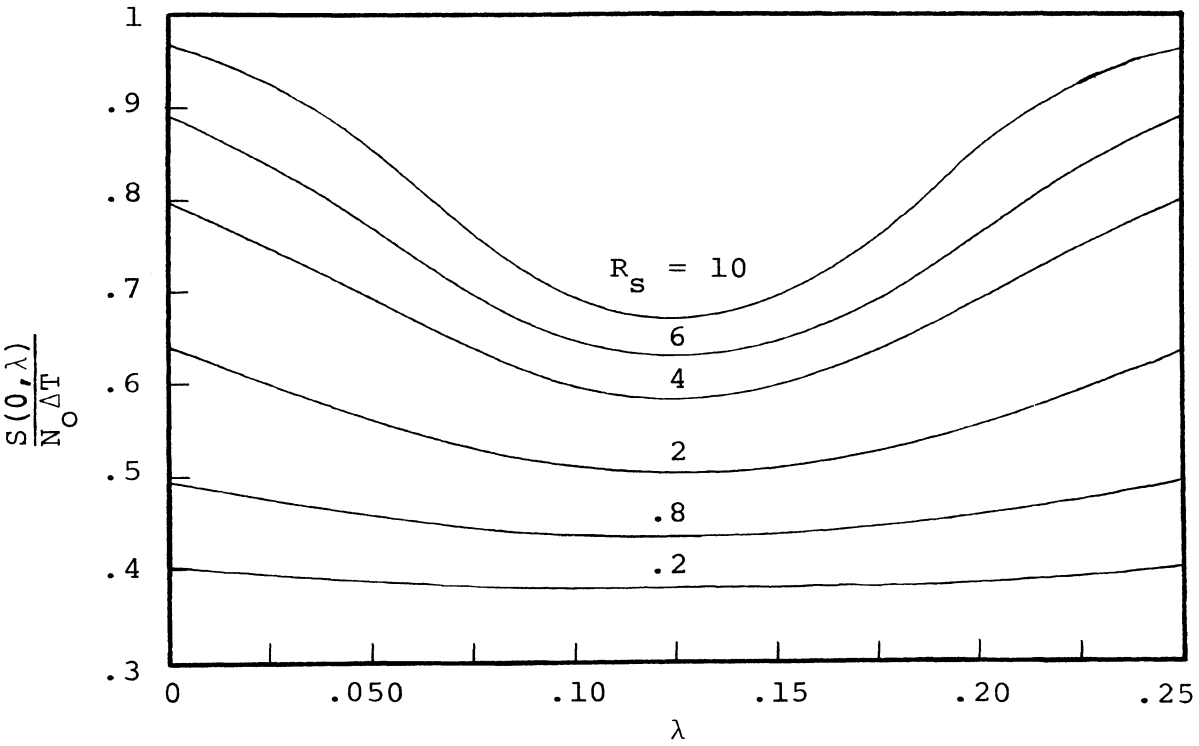

Figure 10. Variation of Equivalent Noise Spectrum with Normalized Phase Error, $\Delta = 1/4$, for AVBS Configuration.

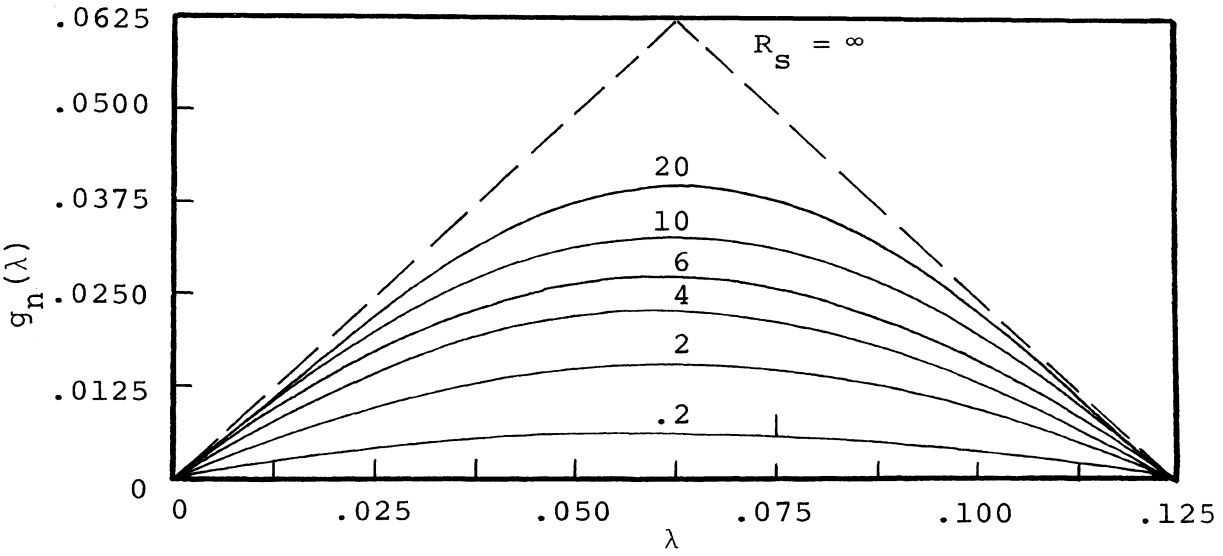

Figure 11. Loop Nonlinearity Versus Normalized Phase Error, $\Delta = 1/8$, for AVBS Configuration.

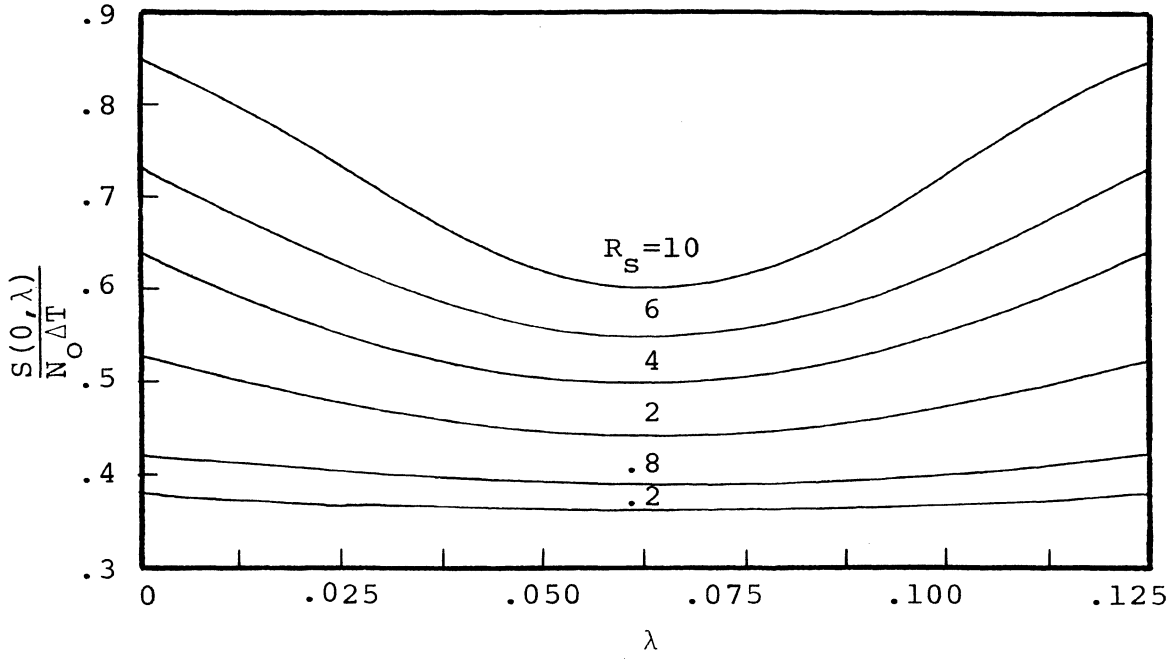

Figure 12. Variation of Equivalent Noise Spectrum With Normalized Phase Error, $\Delta = 1/8$, for AVBS Configuration.

(2) Squaring Loop Type Bit Synchronizer

With reference to Figure 4, the error signal e_k is

$$e_k = (c_k + \nu_k)^2 - (b_k + \mu_k)^2 \tag{15}$$

The evaluation of $g(\lambda)$ is done in Appendix A, with the result

$$g_n(\lambda) = \frac{g(\lambda)}{(AT)^2} = 4(\Delta\lambda - \lambda^2), \quad \lambda \leq \Delta. \tag{16}$$

In this case $g(\lambda)$ is independent of R_s. It can also be shown the $g(\lambda)$ is an odd function of λ. Figure 13 and 15 illustrate the normalized nonlinearity $g_n(\lambda)$, defined above for $\Delta = 1/4$ and $\Delta = 1/8$ cases, respectively.

The computation of $S(\omega,\lambda)$ is done in Appendix B. Since $R(m,\lambda)$ has nonzero value only at $m = 0$, the spectrum consists of a constant component only. $S(\omega,\lambda)$ can be represented by $S(0,\lambda)$. The result is

$$\frac{S(0,\lambda)}{(N_o\Delta T)^2} = h(\lambda) = 1 + 4\Delta R_s + 8\lambda R_s\left(\frac{\lambda}{\Delta} - 1\right), \quad \lambda \leq \Delta. \tag{17}$$

Figure 14 and Figure 16 illustrate the spectrum $S(0,\lambda)$ versus normalized phase error for various values of R_s for $\Delta = 1/4$ and $\Delta = 1/8$, respectively.

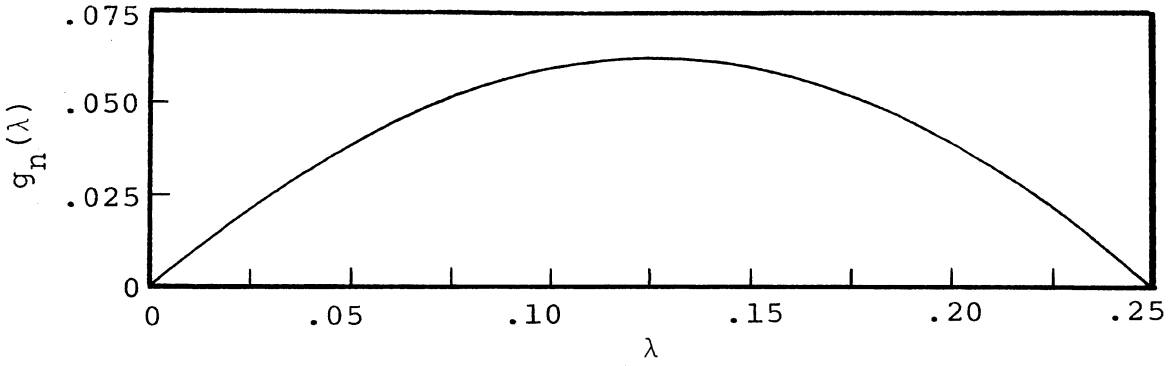

Figure 13. Loop Nonlinearity vs. Normalized Phase Error, Δ = 1/4, SLBS Configuration.

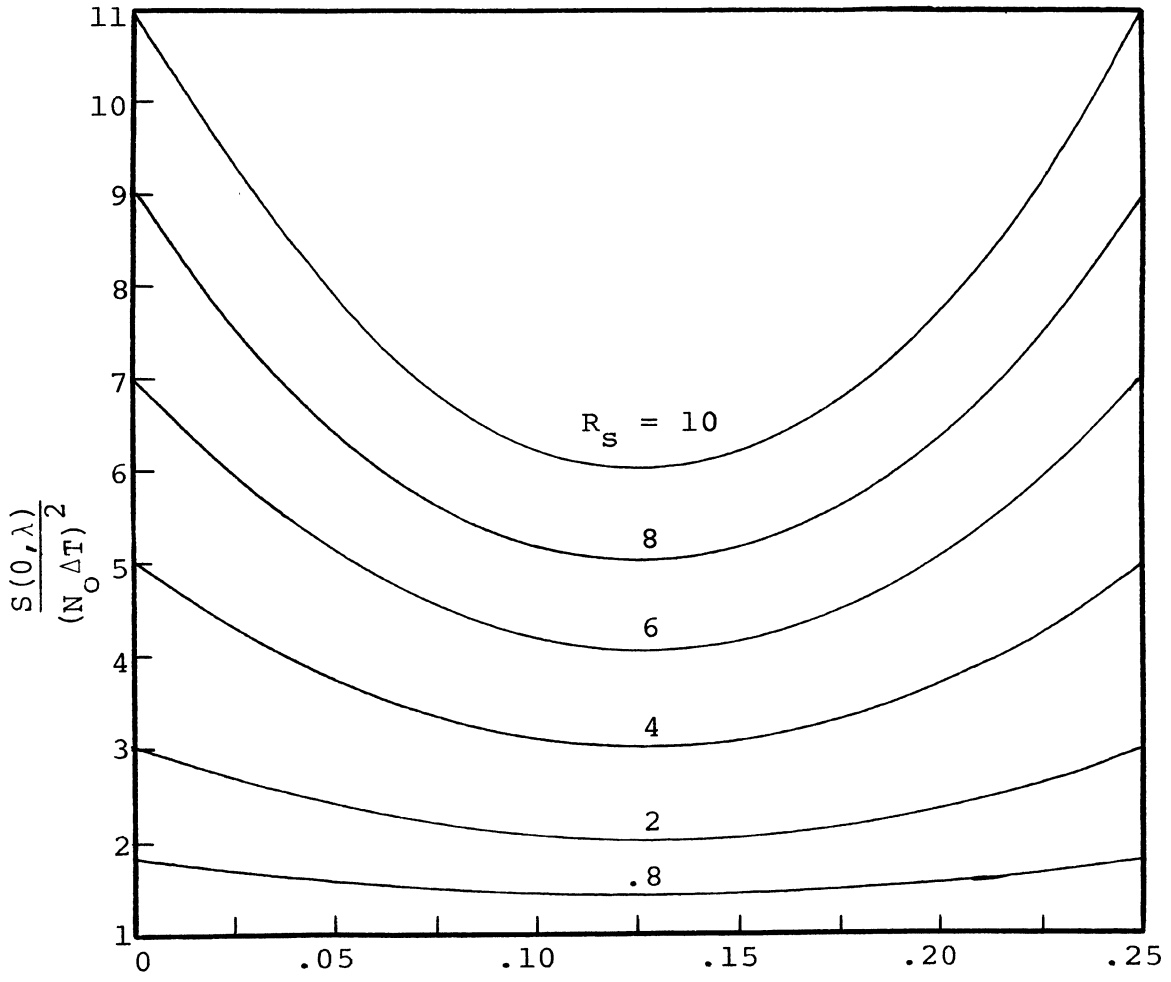

Figure 14. Variation of Equivalent Noise Spectrum With Normalized Phase Error, Δ = 1/4, for SLBS Configuration.

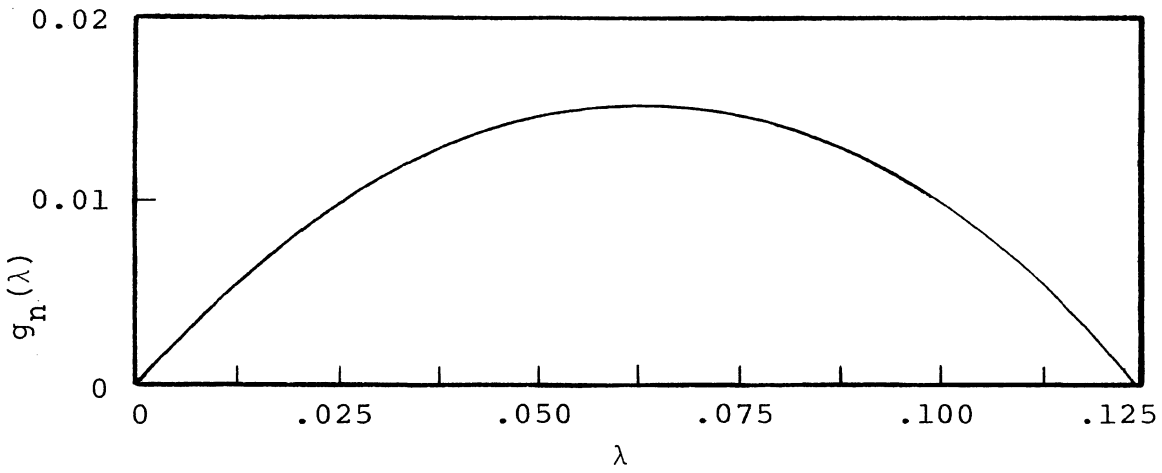

Figure 15. Loop Nonlinearity Versus Normalized Phase Error, $\Delta = 1/8$, for SLBS Configuration.

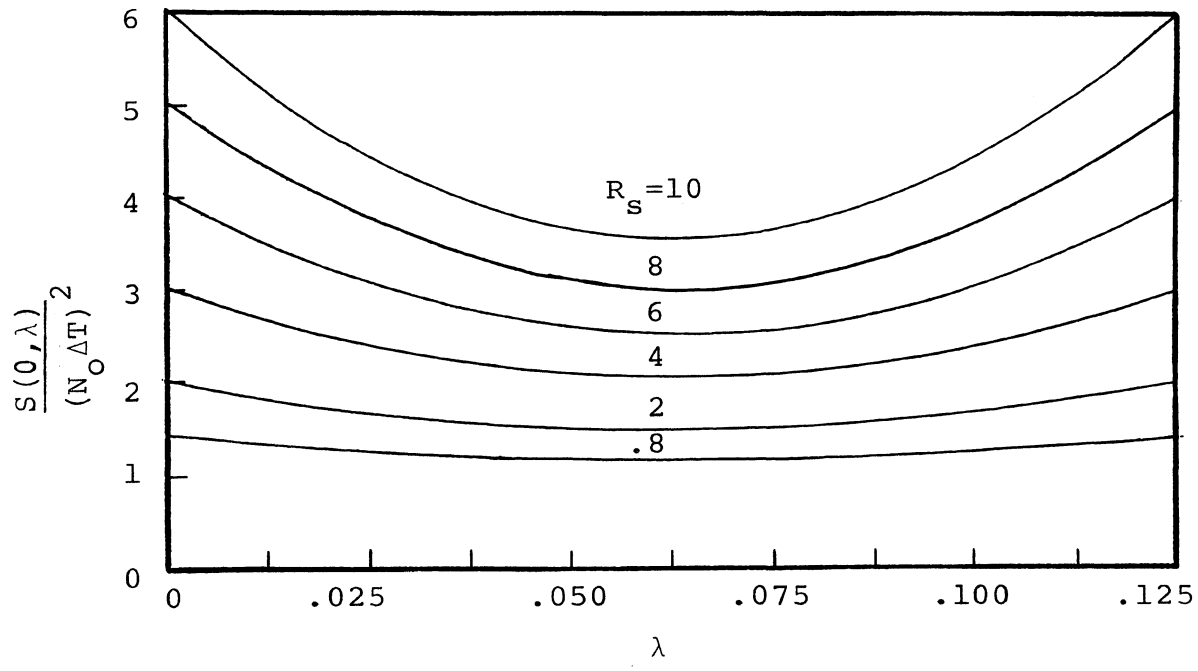

Figure 16. Variation of Equivalent Noise Spectrum with Normalized Phase Error, $\Delta = 1/8$, for SLBS Configuration.

B. Mean Square Phase Noise σ_λ^2 and Probability Density Function of Normalized Phase Error λ

The stochastic differential equation[2] which describes the loop illustrated in Figure 8 is

$$\dot{\lambda} = -K_{VCO}\, F(p)[g\lambda) + n_\lambda(t)] \tag{18}$$

where

p = differential operator d/dt.

In writing the above equation, zero static timing error was assumed. This is consistent with the previous assumption that $\dot{\varepsilon}(t) \doteq 0$.

From Equation (18), the probability distribution of λ, $P(\lambda,t)$, can be found. When the $P(\lambda,t)$ is obtained the mean square phase noise $\sigma_\lambda^2(t)$ can be calculated. If $n_\lambda(t)$ is a white Gaussian process, then the solution for $P(\lambda,t)$ can be found via the Fokker-Planck method. Herein lies the necessity of imposing the Gaussian constraint on $n_\lambda(t)$. The manner in which the method is applied is described in the following. In this study, only the first order case (i.e., $F(p) = K_p$) will be investigated.

It can be reasoned[12] that under the above constraints, the solution to Equation (18), $\lambda(t)$, is a first order Markov process whose probability density function satisfies a diffusion equation[13], namely

$$\frac{\partial P(\lambda,t)}{\partial t} = - \nabla \cdot \underline{W} \tag{19}$$

where in the one dimensional case

$$\underline{W} = W_o = A_o P(\lambda,t) - \frac{1}{2} \frac{\partial}{\partial \lambda} [B_o P(\lambda,t)] \tag{20}$$

A_o and B_o are defined by conditional expectations, i.e.

$$A_o(\lambda_o,t) = \lim_{\Delta t \to 0} \frac{1}{\Delta t} E \left\{ \lambda(t + \Delta t) - \lambda(t) \Big|_{\lambda(t) = \lambda_o} \right\} \tag{21}$$

$$B_o(\lambda_o,t) = \lim_{\Delta t \to 0} \frac{1}{\Delta t} E \left\{ [\lambda(t + \Delta t)] - \lambda(t)]^2 \Big|_{\lambda(t) = \lambda_o} \right\} \tag{22}$$

From Equation (19), the diffusion (or Fokker-Planck) equation describes a flow of probability in phase space. Equation (19) can be rewritten as

$$\frac{\partial P}{\partial t} + \frac{\partial}{\partial \lambda} [A_o P] = \frac{1}{2} \frac{\partial^2}{\partial \lambda^2} [B_o P] . \tag{23}$$

Of particular interest, is the case where $P(\lambda,t)$ converges with time to a stationary probability density function independent of the initial condition. This stationary probability density function may be used to evaluate long-term statistical parameters of the response. In this case

$$\lim_{t \to \infty} \frac{\partial P}{\partial t} = 0$$

Denoting

$$\lim_{t\to\infty} P(\lambda,t) = P_s(\lambda), \tag{24}$$

from Equation (23) the stationary equation is

$$\frac{d}{d\lambda}\left[A_o P_s(\lambda)\right] = \frac{1}{2}\frac{d^2}{d\lambda^2}\left[B_o P_s(\lambda)\right] \tag{25}$$

All that remains is to determine the quantities A_o and B_o. From the definitions in Equations (21) and (22) and the defining loop equation (18),

$$A_o(\lambda) = - K_{VCO}\, K_p\, g(\lambda) \tag{26}$$

$$B_o(\lambda) = (K_{VCO}\, K_p)^2\, S(0,\lambda) \tag{27}$$

The solution to Equation (25) is of the form

$$P_s(\lambda) = c_1 \exp \int_0^{\lambda} \frac{2A_o(y) - \frac{dB_o(y)}{dy}}{B_o(y)}\, dy \tag{28}$$

where C_1 is chosen such that

$$\int_{-\Delta}^{\Delta} P_s(\lambda)\, d\lambda = 1 \tag{29}$$

The mean square phase noise, σ_λ^2, is then given by

$$\sigma_\lambda^2 = \int_{-\Delta}^{\Delta} \lambda^2 P_s(\lambda)\, d\lambda \tag{30}$$

Following the procedure given above, the mean square phase noise, σ_λ^2, of two bit synchronizers under consideration can be evaluated as follows:

(1) Absolute Value Type Bit Synchronizer

Equation (28) when put in terms of the system parameters yields

$$P_s(\lambda) = c_1 \exp\left[-\int_0^{\lambda} \frac{\frac{4R_s\zeta_s K_g}{\Delta} g_n(y) + h'(y)}{h(y)}\, dy\right], \quad \lambda \leq \Delta \tag{31}$$

where

$$\zeta_s = \frac{1}{W_L T}, \qquad W_L = \frac{2AK_{VCO}K_pK_g}{2} \tag{32}$$

K_g = the slope of the normalized S-curve, $g_n(\lambda)$ at $\lambda = 0$

$K_g = \text{erf}(\Delta R_s)^{\frac{1}{2}}$,, for $\Delta = 1/4$ and $1/8$.

C_1 is chosen such that

$$2\int_0^{\Delta} P_s(\lambda)\, d\lambda = 1$$

The prime superscript denotes differentiation.

If $S(0,\lambda)$ is approximated by $S(0,0)$, then Equation (31) reduces to

$$P_s(\lambda) = C_1 \exp\left[-\frac{4R_s\zeta_s K_g}{\Delta h(0)}\int_0^{\lambda} g_n(\lambda)\, dy\right], \quad \lambda \leq \Delta \tag{33}$$

where h(0) from Equation (14) can be found as

$$h(0) = 1 + 2\Delta R_s[1 - (\mathrm{erf}(\Delta R_s)^{\frac{1}{2}})^2] - \frac{2}{\pi}[\exp(-\Delta R_s)]^2$$

$$-4\left(\frac{R_s}{\pi\Delta}\right)[\Delta\,\mathrm{erf}(\Delta R_s)^{\frac{1}{2}}\exp(-\Delta R_s)] \qquad (34)$$

The integral $\int_0^{\lambda} g_n(\lambda)\, d\lambda$ with $g_n(\lambda)$ defined in Equation (12) can be evaluated in closed form and is done in Appendix C with the result

$$\int_0^{\lambda} g_n(\lambda)\, d\lambda = \frac{1}{2}\{(\Delta\lambda - \frac{\Delta}{8R_s} - \frac{\Delta^2}{4})\,\mathrm{erf}(\Delta R_s)^{\frac{1}{2}} +$$

$$+ (\frac{\Delta}{8R_s} + \frac{(\Delta - 2\lambda)^2}{4}).$$

$$\mathrm{erf}\left(\frac{(\Delta - 2\lambda)R_s^{\frac{1}{2}}}{\Delta^{\frac{1}{2}}}\right) + [(\frac{\Delta\lambda^2}{\pi R_s})^{\frac{1}{2}} - 0.25(\frac{\Delta^3}{\pi R_s})^{\frac{1}{2}}].$$

$$\exp(-\Delta R_s) + \frac{\Delta^{\frac{1}{2}}(\Delta - 2\lambda)}{4(\pi R_s)^{\frac{1}{2}}} \cdot \exp(-\frac{(\Delta - 2\lambda)^2 R_s}{\Delta})\}$$

$$,\lambda \leq \Delta. \qquad (35)$$

C_1 can be solved numerically using Romberg's Method of numerical integration.

The mean square phase noise, σ_λ^2, is then given by

$$\sigma_\lambda^2 = 2\int_0^{\Delta} \lambda^2 P_s(\lambda)\, d\lambda \qquad (36)$$

Equation (36) can be solved numerically using Romberg's Method of numerical integration. Figure 17 and Figure 18 show σ_λ^2 versus R_s by neglecting the variation of the noise spectrum with phase error, at $\zeta_s = 10$ and 50 for $\Delta = 1/4$ and $\Delta = 1/8$ cases, respectively.

By evaluating Equation (33) and Equation (36) several results are observed, namely:

a. For small $R_s\zeta_s$, the distribution $P_s(\lambda)$ becomes uniform in the interval $(-\Delta, \Delta)$. In fact

$$\lim_{R_s \to 0} \sigma_\lambda^2 = \frac{1}{48} \quad \text{for } \Delta = 1/4 \tag{37}$$

$$\lim_{R_s \to 0} \sigma_\lambda^2 = \frac{1}{192} \quad \text{for } \Delta = 1/8 \tag{38}$$

b. For large $R_s\zeta_s$, $P_s(\lambda)$ approaches a zero mean distribution of the form

$$P_s(\lambda) = C_1 \exp\left(-\frac{4R_s\zeta_s\lambda^2}{2\Delta}\right), \quad \lambda \leq \Delta. \tag{39}$$

with variance determined in Appendix D, with the result

$$\sigma_\lambda^2 = \frac{\Delta}{4R_s\zeta_s} \tag{40}$$

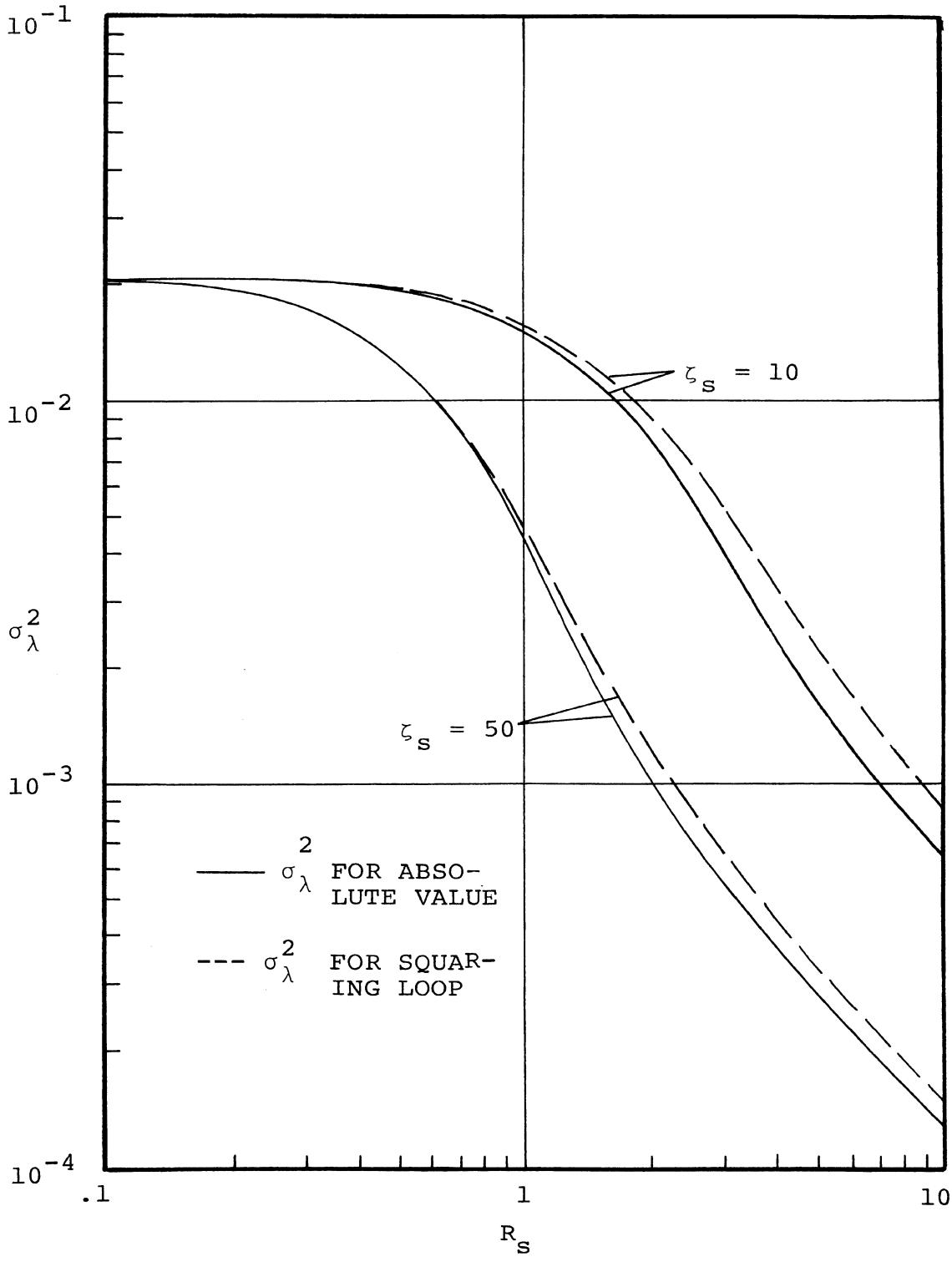

Figure 17. A Comparison of the Phase Noise Performance of AVBS and SLBS Configurations for $\Delta = 1/4$ (Same Loop Bandwidth).

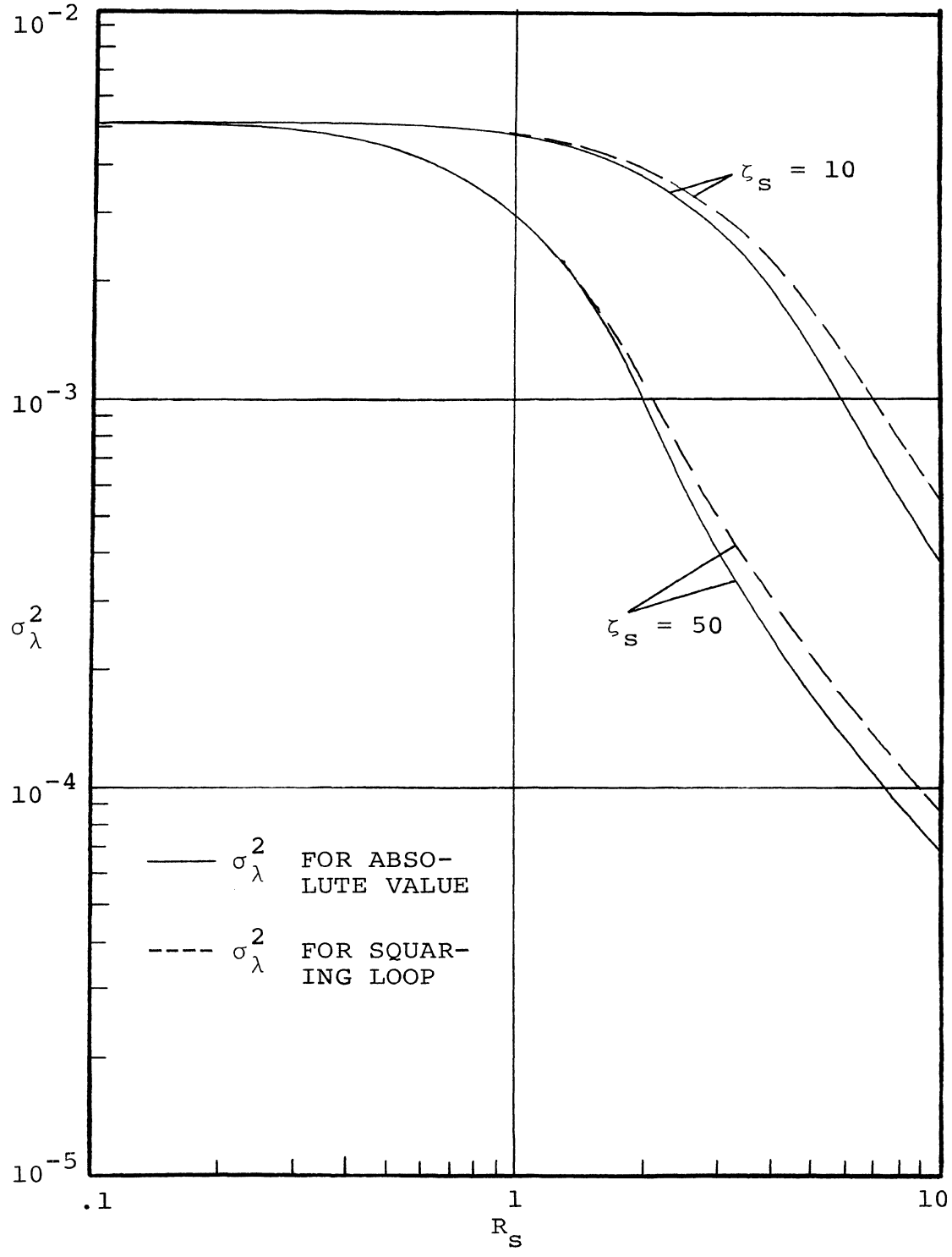

Figure 18. A Comparison of the Phase Noise Performance of AVBS and SLBS Configurations for $\Delta = 1/8$ (Same Loop Bandwidth).

c. For other values of $R_s\zeta_s$ the distribution of λ is in continuous transition between the two limiting cases of a. and b. Figure 19 illustrates this transitional behavior as R_s varies at fixed $\zeta_s = 10$ for $\Delta = 1/4$.

2. Squaring Loop Type Bit Synchronizer

Equation (28) when put in terms of the system parameters yields

$$P_s(\lambda) = C_1 \exp\left[-\int_0^{\lambda} \frac{\frac{R_s^2\zeta_s K_g}{\Delta^2} g_n(y) + h'(y)}{h(\lambda)}\, dy\right], \quad \lambda \leq \Delta \tag{41}$$

where

$$\zeta_s = \frac{1}{W_L T} \quad , \quad W_L = \frac{A^2 T K_{VCO} K_p K_g}{2} \tag{42}$$

K_g = the slope of the normalized S-curve, $g_n(\lambda)$ at $\lambda = 0$

$K_g = 1$, for $\Delta = 1/4$, $K_g = 1/2$ for $\Delta = 1/8$

C_1 is chosen such that

$$2\int_0^{\Delta} P_s(\lambda)\, d\lambda = 1$$

The prime superscript denotes differentiation

If $S(0,\lambda)$ is approximated by $S(0,0)$, then Equation (41) reduces to

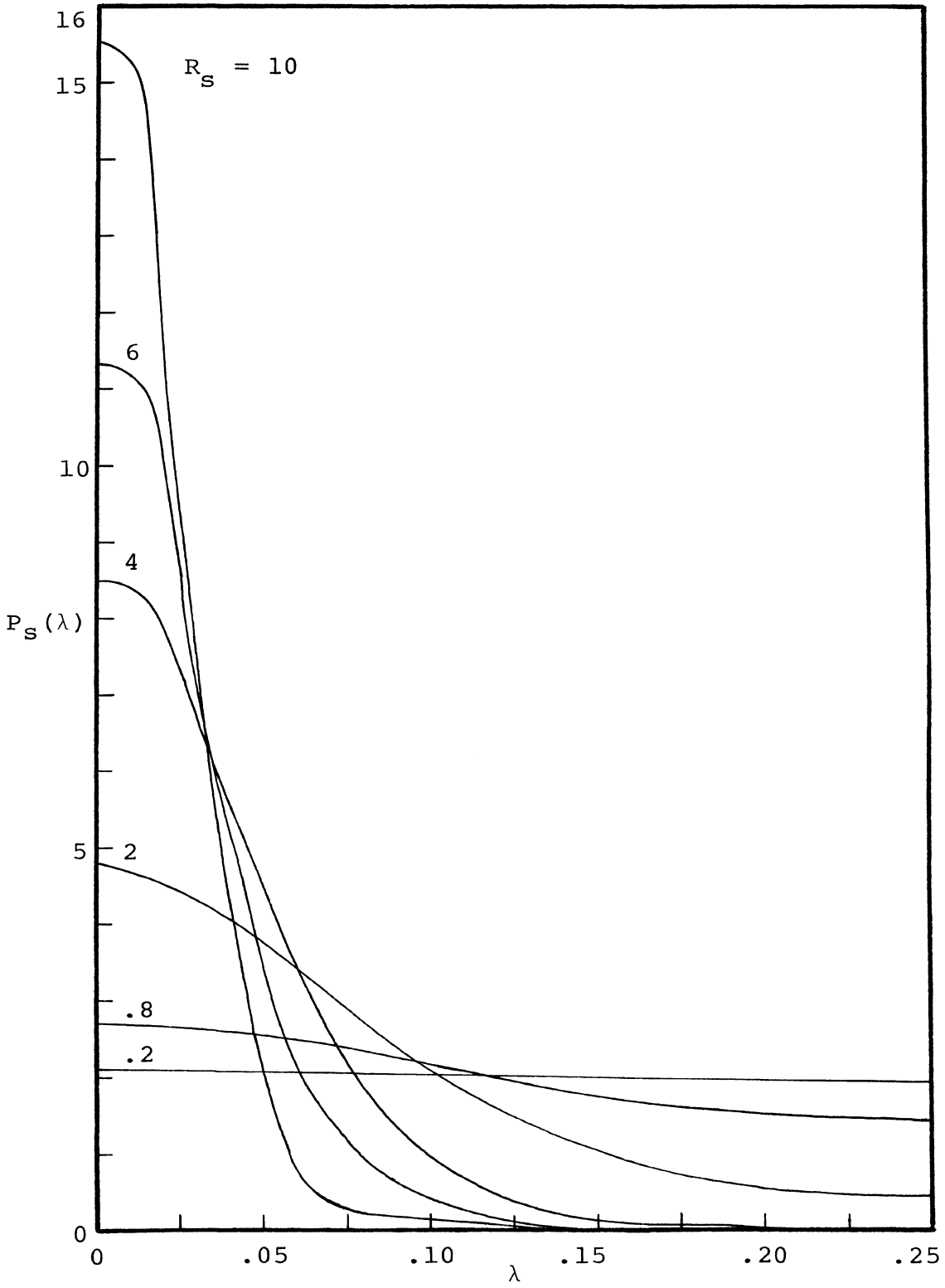

Figure 19. Probability Distribution of Normalized Phase Error For AVBS Configuration, ζ_s = 10 and Δ = 1/4.

$$P_s(\lambda) = C_1 \exp\left[-\frac{R_s^2 \zeta_s K_g}{\Delta^2 h(0)} \int_0^{\lambda} g_n(\lambda)\, dy\right], \quad \lambda \leq \Delta \tag{43}$$

where $h(0)$ from Equation (17) can be found as

$$h(0) = 1 + 4\Delta R_s \tag{44}$$

The integral $\int_0^{\lambda} g_n(\lambda)\, d\lambda$ with $g_n(\lambda)$ in Equation (16) can be evaluated with the result

$$\int_0^{\lambda} g_n(\lambda)\lambda d = 2\Delta\lambda^2 - \frac{4}{3}\lambda^3, \quad \lambda \leq \Delta \tag{45}$$

C_1 can be solved numerically using Romberg's method of numerical integration.

The mean square phase noise, σ_λ^2, is then given by

$$\sigma_\lambda^2 = 2 \int_0^{\Delta} \lambda^2 P_s(\lambda)\, d\lambda \tag{46}$$

Equation (46) can be solved numerically using Romberg's method of numerical integration.. Figure 17 and Figure 18 show σ_λ^2 versus R_s by neglecting the variation of the noise spectrum with phase error, at ζ_s = 10 and 50 for Δ = 1/4 and Δ = 1/8 cases, respectively.

By evaluating Equation (43) and Equation (46) several results are observed, namely;

a. For small $R_s\zeta_s$, the distribution $P_s(\lambda)$ becomes uniform in the interval $(-\Delta,\Delta)$. In fact

$$\lim_{R_s\to 0} \sigma_\lambda^2 = \frac{1}{48} \quad , \text{ for } \Delta = 1/4 \tag{47}$$

$$\lim_{R_s\to 0} \sigma_\lambda^2 = \frac{1}{192} \quad , \text{ for } \Delta = 1/8 \tag{48}$$

b. For large $R_s\zeta_s$, $P_s(\lambda)$ approaches a zero mean Gaussian distribution.

c. For other values of $R_s\zeta_s$ the distribution of λ is in continuous transition between the two limiting cases of a. and b. Figure 20 illustrates this transitional behavior as R_s varies at $\zeta_s = 10$ for $\Delta = 1/4$.

C. Probability of Bit-Detection Error

As mentioned previously, the bit detection portion is common to both bit synchronizers under investigation. It is now necessary to investigate the effects of phase error on the output SNR due to extracted timing information from bit synchronization portion. With reference to Figure 7b, the switching effects on Sø to NRZ conversion can be found. When there are two successive 1's or 0's, there will be two notches per information pulse, one near the center and one at the end. When there are alternate

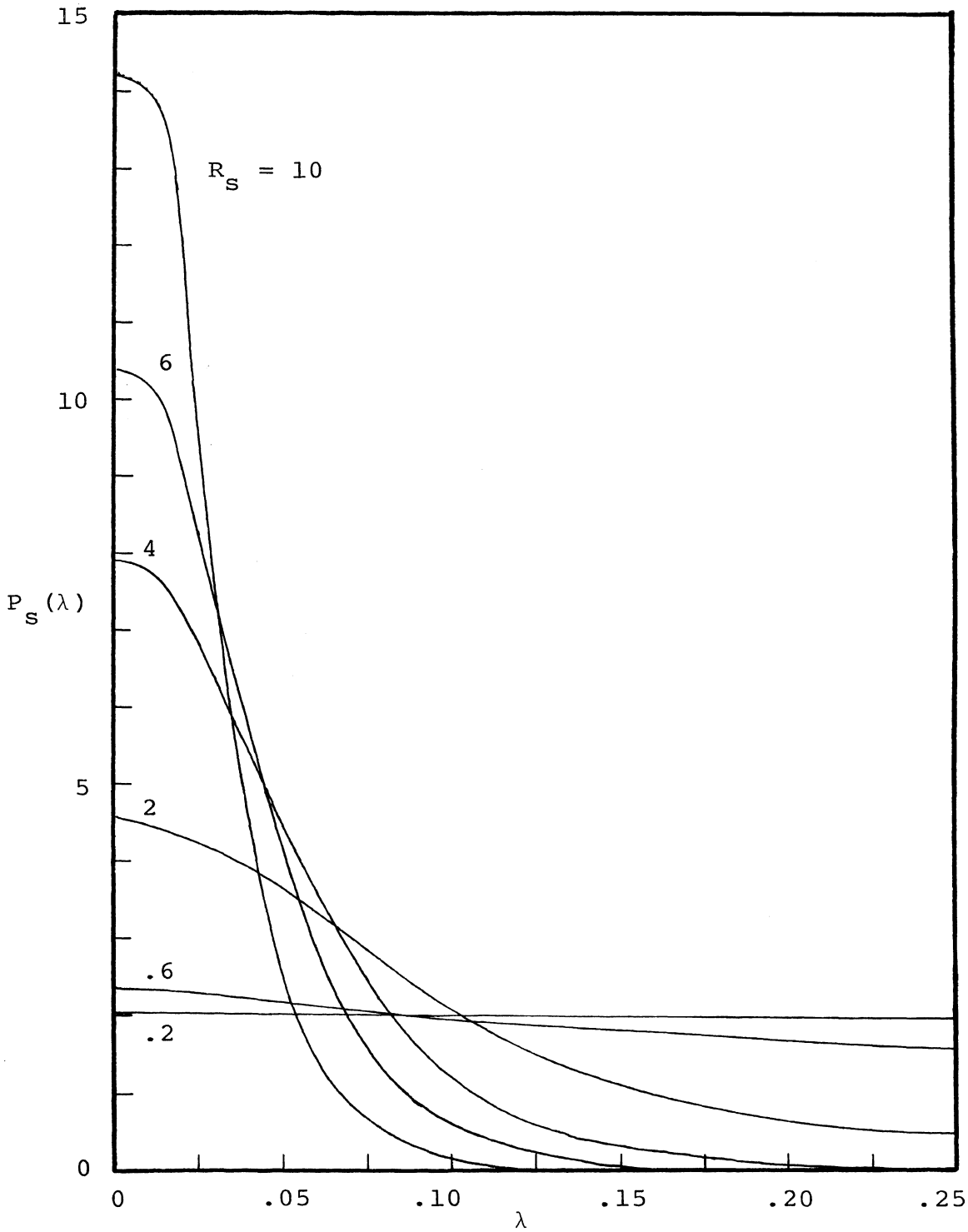

Figure 20. Probability Distribution of Normalized Phase Error for SLBS Configuration, $\zeta_s = 10$ and $\Delta = 1/4$.

1 and 0, there will be one notch near the center of the information bit. The results are essentially the same for negative or late timing errors. With reference to Figure 7b, the combined effects of the switching and sampling errors due to imperfect early timing can be seen. Assuming the integrator starts to build up early by λT. During this build-up process, a notch occurs due to switching, causing the integrator to reverse the direction of integration. At the end of the notch, the integrator starts to integrate positively. The switching notch at the end of the information causes the integrator to again reverse direction until it is finally dumped. The amplitude for this first integrator output is $A(1 - 4\lambda)$.

The four errors occur as follows. One error due to early integration; two errors due to the integrator reversal in the middle of the information bit; and one error due to the integrator reversal at the end of the information bit.

On the second pulse, the integrator starts early again. There is a reversal of the integrator in the middle due to a switching error. The switching error at the end of this second information bit produces an elongation rather than a notch. Since the sampling pulse is early, the integrator continues its negative build-up until it is dumped. This additional build-up cancels one of the

timing errors. Therefore, the resulting amplitude factor is $(1 - 2\lambda)$. It follows that when there is a polarity reversal at the end of the previous information bit, there are two timing errors. This is true for either late or early timing errors.

From the above investigation, an expression for the signal-to-noise ratio corresponding to any sampling pulse for equal 1 and 0 probabilities can be obtained

$$\rho = \begin{cases} (1 - 4|\lambda|)^2 R_s; \text{ with probability } 1/2, \\ (1 - 2|\lambda|)^2 R_s; \text{ with probability } 1/2. \end{cases} \quad (49)$$

With the effects of phase error on the output SNR due to extracted timing information obtained, the probability of error $P(\varepsilon|\lambda)$, conditional on knowing λ, can be found as follows.

$$P(\varepsilon|\lambda) = \frac{1}{2} P(z \geq \sqrt{\rho}|\lambda, C) + \frac{1}{2} P(z \geq \sqrt{\rho}|\lambda, D), \quad \lambda \leq \Delta \quad (50)$$

where C refers to successive 1's or 0's, and D refers to successive 1 - 0 reversals. From Equation (49).

$$P(z \geq \sqrt{\rho}|\lambda, C) = P(z \geq (1 - 4|\lambda|)\sqrt{R_s}|\lambda, C)$$

$$= \int_{(1 - 4|\lambda|)\sqrt{R_s}}^{\infty} \frac{1}{\sqrt{\pi}} e^{-z^2} dz = \frac{1}{2} \operatorname{erfc}((1 - 4|\lambda|)\sqrt{R_s}),$$

$$\lambda \leq \Delta. \quad (51)$$

where erfc(z) is the complementary error function. Similarly

$$P(z \geq \sqrt{\rho}\,|\lambda, D) = \frac{1}{2}\,\mathrm{erfc}((1 - 2|\lambda|)\sqrt{R_s}),\ \lambda \leq \Delta. \qquad (52)$$

Applying Equations (51) and (52) to Equation (50),

$$P(\varepsilon|\lambda) = \frac{1}{4}\,\mathrm{erfc}((1 - 4|\lambda|)\sqrt{R_s}) + \frac{1}{4}\mathrm{erfc}((1 - 2|\lambda|)\sqrt{R_s}) \qquad (53)$$

The probability of bit-detection error $P(\varepsilon)$ is

$$P(\varepsilon) = \int_{-\Delta}^{\Delta} P(\varepsilon|\lambda)\ P_s(\lambda)\ d\lambda$$

$$= \frac{1}{4}\int_{-\Delta}^{\Delta} \{P_s(\lambda)\ [\mathrm{erfc}((1 - 4|\lambda|)\sqrt{R_s})$$

$$+ \mathrm{erfc}((1 - 2|\lambda|)\sqrt{R_s})]\}\ d\lambda \qquad (54)$$

where $P_s(\lambda)$ is defined in Equation (33) for AVBS case and in Equation (43) for SLBS case.

Evaluation of Equation (54) requires numerical integration. The results versus various R_s for AVBS case and SLBS case are plotted in Figure 21 and Figure 22 at ζ_s = 10 and 50 for Δ = 1/4 and Δ = 1/8, respectively.

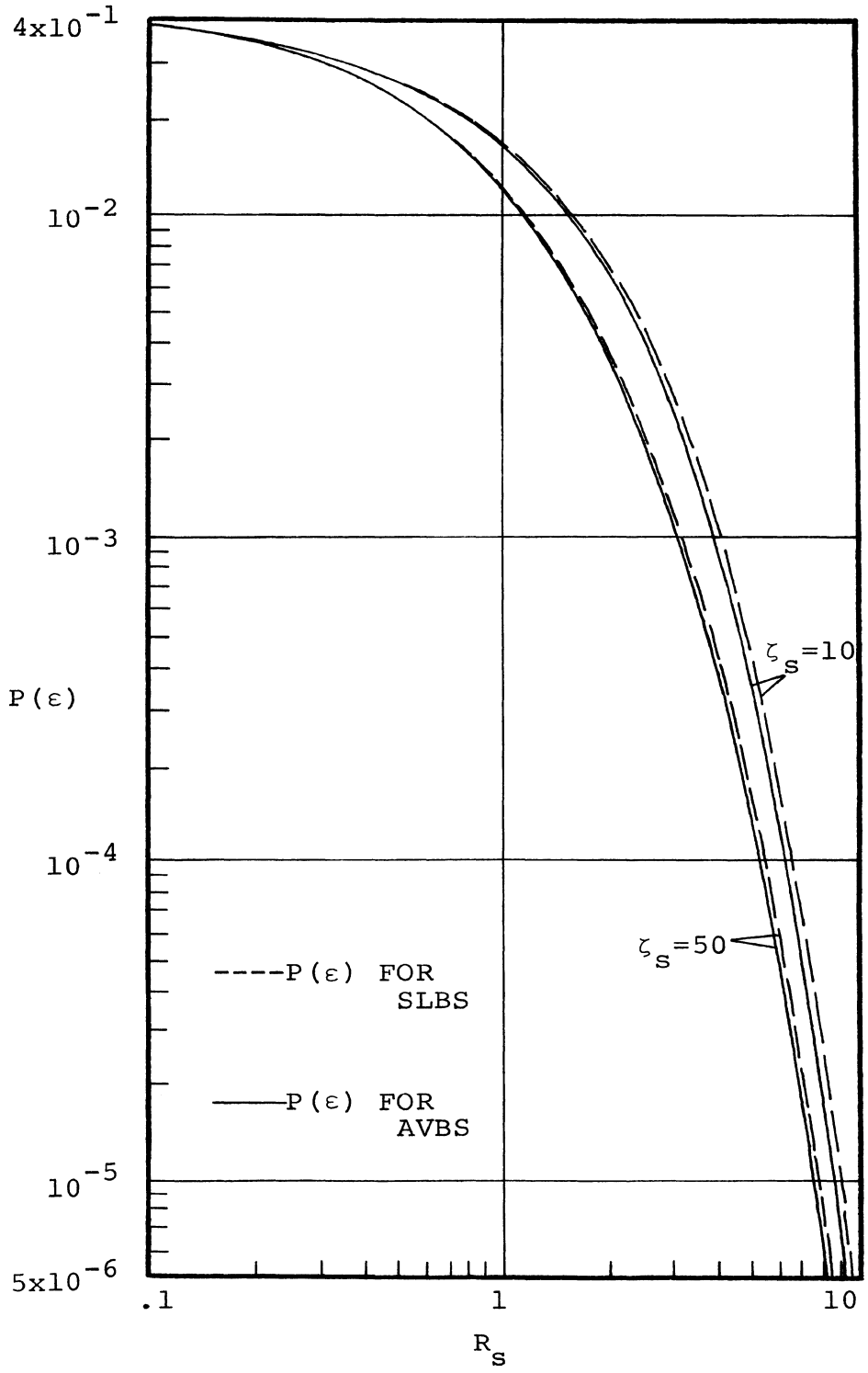

Figure 21. A Comparison of the Probability of Bit-Detection Error of AVBS and SLBS Configurations for $\Delta = 1/4$.

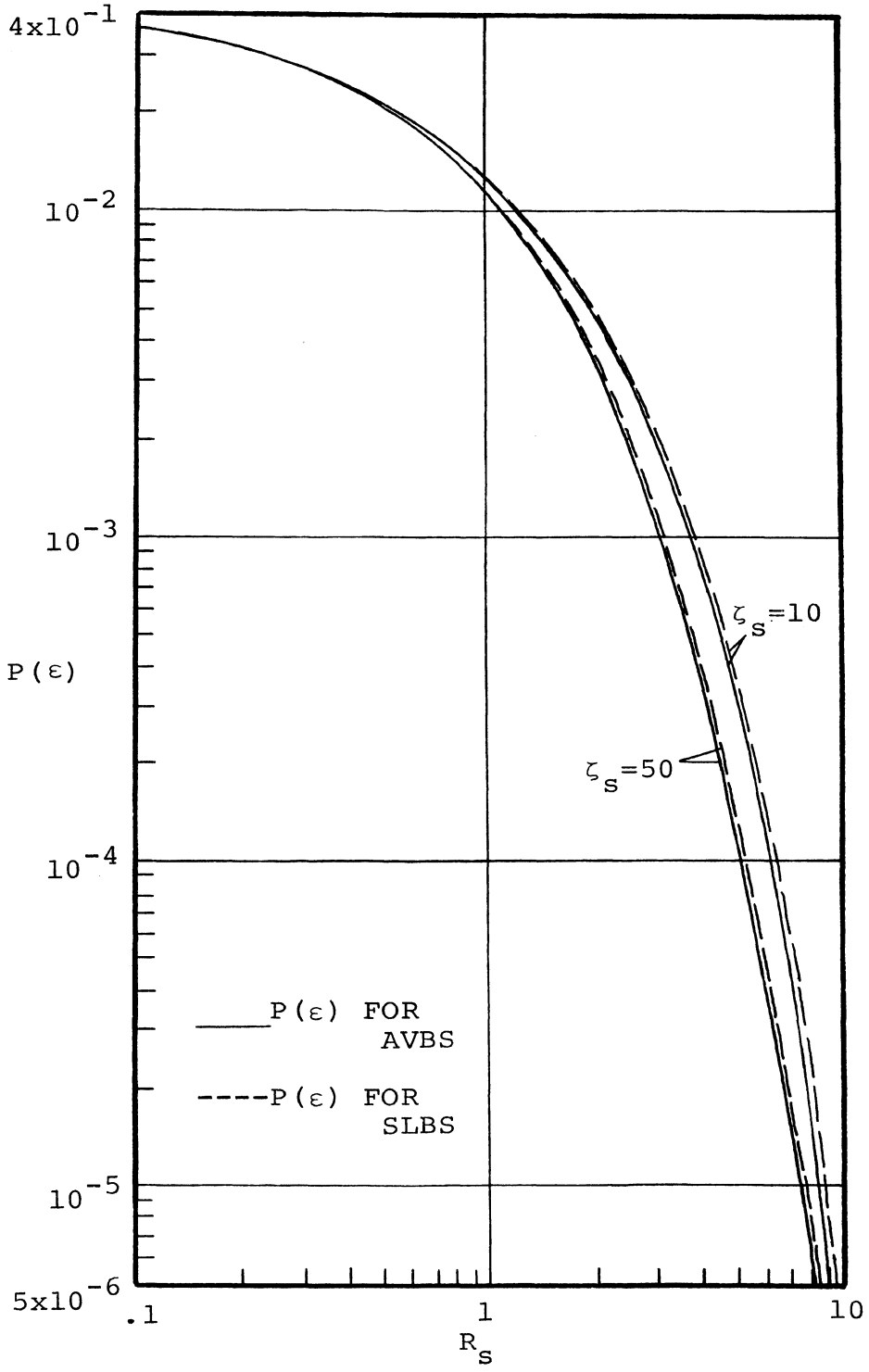

Figure 22. A Comparison of the Probability of Bit-Detection Error of AVBS and SLBS Configurations for $\Delta = 1/8$.

V. RESULTS AND CONCLUSIONS

The analysis of the two bit synchronizer configurations began by evaluating the loop nonlinearity, $g(\lambda)$, and the spectrum of additive noise, $S(\omega,\lambda)$. An equivalent phase-locked loop was formed by employing these two quantities. By applying the Fokker-Planck technique, the probability distributions of the normalized phase error and the mean square noise, σ_{λ}^{2}, of the two bit synchronizer configuration for $\Delta = 1/4$ and $\Delta = 1/8$ modes were evaluated. Finally the probability of bit-detection errors were evaluated.

It was found that, while the phase jitter was less than one-eighth of a bit interval, both bit synchronizer configurations in the $\Delta = 1/8$ mode offered a 6 dB and a 3 dB phase noise advantage over those in the $\Delta = 1/4$ mode for $R_s\zeta_s$ small and $R_s\zeta_s$ large cases, respectively. As for the comparison of the mean square phase errors on the basis of equal loop bandwidth between two bit synchronizer configurations, the following was found.

a. When $R_s\zeta_s$ was small, the mean square phase error of the AVBS configuration and the SLBS configuration were equal for both $\Delta = 1/4$ and $\Delta = 1/8$ modes.

b. When $R_s\zeta_s$ was large, the AVBS configuration offered a .66 dB and a .79 dB phase noise advantage over the SLBS configuration for $\Delta = 1/4$ and $\Delta = 1/8$ modes, respectively.

c. For other values of $R_s\zeta_s$, the comparisons were made in Figure 17 and Figure 18 for $\Delta = 1/4$ and $\Delta = 1/8$ modes, respectively. It was found that the phase noise in these regions of the AVBS configuration were always smaller than that of the SLBS configuration.

The comparison of the overall performance for the two modes or the two bit synchronizer configurations could be made by comparing the probability of bit-detection errors of the systems. It was found that, while the phase jitter was less than one-eighth of a bit interval, both bit synchronizer configurations in the $\Delta = 1/8$ mode offered a .37 dB and a 10.9 dB advantage over the $\Delta = 1/4$ mode for $R_s\zeta_s$ small and $R_s\zeta_s$ large cases, respectively. The comparison between two bit synchronizer configurations for two modes was found as follows.

a. When $R_s\zeta_s$ was small, the probability of bit-detection errors of the AVBS configuration and the SLBS configuration were equal for both $\Delta = 1/4$ and $\Delta = 1/8$ modes.

b. When $R_s\zeta_s$ was large, the probability of bit-detection error of the AVBS configuration offered a .3dB and a .25 dB advantage over the SLBS configuration for $\Delta = 1/4$ and $\Delta = 1/8$ modes respectively.

c. For other values of $R_s\zeta_s$, the comparisons were made in Figure 21 and Figure 22 for $\Delta = 1/4$ and $\Delta = 1/8$ modes, respectively. It was found that the probability of bit-detection errors in these regions of the AVBS configuration were always smaller than that of the SLBS configuration.

From the comparisons made above, it can be concluded that the performance of the AVBS configuration is better than that of the SLBS configuration.

VI. FUTURE AREAS OF INVESTIGATION

1. Mean-square phase jitter and probability of bit-detection error for higher-order systems (i.e., higher-order filters)
2. Mean time to first slip or equivalently mean frequency of skipped cycles for first and higher order systems
3. Experimental varification or digital computer simulation of the above results
4. Limiting performance for $W_L T$ in the neighborhood of unity.

REFERENCES

1. C. Carl, "Relay Telemetry Modulation System Development," Jet Propulsion Lab., Pasadena, Calif., Space Programs Summary 37-50, Vol. 3, pp. 326-331.

2. P. A. Wintz, and E. J. Luecke, "Performance of Self-Bit Synchronization Systems," Report made under NASA Grant NsG-553, School of Electrical Engineering, Purdue University, June 1968.

3. W. C. Lindsey, and R. C. Tausworthe, "Digital Data-Transition Tracking Loops," Jet Propulsion Lab., Pasadena, Calif., Space Programs Summary 37-50, Vol. 3, pp. 272-276.

4. Marvin K. Simon, "An Analysis of the Steady-State Phase-Noise Performance of a Digital-Data-Trancition Tracking Loop," Jet Propulsion Lab., Pasadena, Calif., Space Programs Summary 37-55, Vol. 3, pp. 54-62.

5. W. C. Lindsey, and Tage O. Anderson, "Digital-Data-Transition Tracking Loops," Proceedings of the 1968 International Telemetry Conference, October 1968, pp. 259-271.

6. J. J. Stiffler, "On the Performance of a Class of PCM Bit Synchronizers," Proceedings of the National Telemetry Conference, April 1969, pp. 67-70.

7. J. W. Layland, "Telemetry Bit Synchronization Loop," Jet Propulsion Lab., Pasadena, Calif., Space Programs Summary 37-46, Vol. 3, pp. 204-215.

8. Marvin K. Simon, "Nonlinear Analysis of an Absolute Value Type of an Early-Late Gate Bit Synchronizer," IEEE Transactions on Communication Technology, October 1970, pp. 589-596.

9. A. G. Glenn, and G. Lieberman, "Effect of Noise Synchronization Signals on Split-phase Coded System Performance," RCA Review, December 1969, pp. 595-608.

10. Alan L. McBride, and Andrew P. Sage, "Optimum Estimation of Bit Synchronization," IEEE Transactions on Aerospace and Electronic System, May 1969, pp. 525-536.

11. A. J. Viterbi, Principles of Coherent Communication, McGraw-Hill, 1966, pp. 35-36.

12. Athanasios Papoulis, Probability, Random Variables, and Stochastic Processes, McGraw-Hill, 1965, pp. 536-538.

13. IBID., pp. 538-542.

VITA

Kuang-Cheng Hu was born on February 15, 1942, in Chungking, China. He received his primary and secondary education in Taipei, Taiwan, Republic of China. He received his diploma in Electrical Engineering from Taiwan Provincial Taipei Institute of Technology, in Taipei, Republic of China, in June 1961. After graduation from that institute, he served in the Chinese Navy as an Ensign for one year. Then he worked in the industries in Taiwan for five years. In August 1968 he came to the United States to enroll in the Electrical Engineering Department of the University of Missouri-Rolla, in Rolla, Missouri. He received his Bachelor of Science degree in Electrical Engineering from the University of Missouri-Rolla in January 1970. He has been enrolled in the Graduate School of the University of Missouri-Rolla since that time.

APPENDIX A

Evaluation of the Loop Nonlinearity $g(\lambda)$

(1) Absolute Value Type Early-Late-Gate-Integration Type of Bit Synchronizer

To evaluate $g(\lambda)$ defined by Equation (7) of the main text, and considering first the average with respect to noise,

$$E_n\{e_k\} = E_n\{c_k \operatorname{sgn}(c_k + \nu_k) + \nu_k \operatorname{sgn}(c_k + \nu_k)\}$$

$$- E_n\{b_k \operatorname{sgn}(b_k + \mu_k) + \mu_k \operatorname{sgn}(b_k + \mu_k)\}$$

But,

$$E_n\{\operatorname{sgn}(c + y)\} = \operatorname{erf}\left(\frac{c}{\sqrt{2}\sigma_y}\right) \qquad \text{(A-1.1)}$$

where

$$\operatorname{erf} z = \frac{2}{\sqrt{\pi}} \int_0^z e^{-t^2}\, dt$$

and

$$E_n\{y \operatorname{sgn}(c + y)\} = \sqrt{2/\pi}\, \sigma_y \exp\left(-\frac{c^2}{2\sigma_y^2}\right) \qquad \text{(A.1.2)}$$

Thus

$$E_n\{e_k\} = c_k \operatorname{erf}\left(\frac{c_k}{\sqrt{2}\sigma_\nu}\right) - b_k \operatorname{erf}\left(\frac{b_k}{\sqrt{2}\sigma_\mu}\right)$$

$$+\sqrt{2/\pi}\, \sigma\left\{\exp\left(-\frac{c_k^2}{2\sigma_\nu^2}\right) - \exp\left(-\frac{b_k^2}{2\sigma_\mu^2}\right)\right\} \qquad \text{(A.1.3)}$$

It now remains to average $E_n\{e_k\}$ over the signal distribution. From

$$c_k = \int_{(k+\frac{1}{2}-\Delta-\lambda)T}^{(k+\frac{1}{2}-\lambda)T} s(t)\,dt$$

$$= \int_{(k+\frac{1}{2}-\Delta-\lambda)T}^{(k+\frac{1}{2}-\lambda)T} d_k\, P(t - kT - \varepsilon(t))\,dt = \Delta T d_k$$

$$b_k = \int_{(k+\frac{1}{2}-\lambda)T}^{(k+\frac{1}{2}+\Delta-\lambda)T} s(t)\,dt$$

$$= \int_{(k+\frac{1}{2}-\Delta)T}^{(k+\frac{1}{2})T} d_k\, p(t - kT - \varepsilon(t))\,dt$$

$$- \int_{(k+\frac{1}{2})T}^{(k+\frac{1}{2}+\Delta-\lambda)T} d_k\, p(t - (k+\tfrac{1}{2})T - \varepsilon(t))\,dt$$

$$= \lambda T d_k - (\Delta - \lambda) T d_k \qquad \text{(A-1.4)}$$

where d_i is again the i^{th} input symbol, taking on values $\pm A$ with equal probability. Substituting (A-1.4) in (A-1.3), and averaging over all possible equally likely outcomes of the symbol d_k, it results

$$g_n(\lambda) = \frac{g(\lambda)}{2AT} = \frac{1}{2}\{\Delta \operatorname{erf}(\sqrt{\Delta R_s}) - (\Delta - 2\lambda)\operatorname{erf}[(\Delta - 2\lambda)\sqrt{R_s}/\Delta]$$

$$+ \sqrt{\Delta/\pi R_s}\,[\exp(-\Delta R_s) - \exp(-\frac{(\Delta - 2\lambda)^2 R_s}{\Delta})]\},\lambda \leq \Delta. \quad \text{(A-1.5)}$$

(2) Squaring Loop Type Early-Late-Gate-Integration Type of Bit Synchronizer

To evaluate $g(\lambda)$ define Equation (7) of the main text, and considering first the average with respect to the noise.

$$E_n\{e_k\} = E_n\{(c_k + \nu_k)^2 - (b_k + \mu_k)^2\}$$

$$= c_k^2 - b_k^2 \quad \text{(A-2.1)}$$

It now remains to average $E_n\{e_k\}$ over the signal distributions. Substituting (A-1.4) in (A-2.1), and averaging over all possible equally likely outcomes of the symbol d_k, yields

$$g_n(\lambda) = \frac{g(\lambda)}{(AT)^2} = 4(\Delta\lambda - \lambda^2)\ ,\ \lambda \leq \Delta. \quad \text{(A-2.2)}$$

APPENDIX B

Evaluation of the Loop Spectrum, $S(\omega,\lambda)$

(1) Absolute Value Type Early-Late-Gate-Integration Type of Bit Synchronizer

To evaluate $S(\omega,\lambda)$ defined by Equation (10) of the main text, the first term is given below

$$E_{n,s}\{e_k e_{k+m}|\lambda\} = E_{n,s}\{[(c_k + \nu_k)\operatorname{sgn}(c_k + \nu_k) - (b_k + \mu_k)\operatorname{sgn}(b_k + \mu_k)][(c_{k+m} + \nu_{k+m})\operatorname{sgn}(c_{k+m} + \nu_{k+m}) - (b_{k+m} + \mu_{k+m})\operatorname{sgn}(b_{k+m} + \nu_{k+m})]|\lambda\} \quad \text{(B-1.1)}$$

When $m \neq 0$

ν_k, ν_{k+m}, μ_k, μ_{k+m} are all mutually statistically independent

c_k and c_{k+m} are mutually statistically independent for all k and m

b_k and b_{k+m} are mutually statistically independent for all k and m

c_k and b_{k+m} are mutually statistically independent for all k and m

b_k and c_{k+m} are mutually statistically independent for all k and m

c_k and b_k are mutually statistically independent for all k

so e_k and e_{k+m} are mutually statistically independent random variables.

Equation (B-1.1) yields

$$E_{n,s}\{e_k e_{k+m}|\lambda\} = E_{n,s}\{e_k|\lambda\}\, E_{n,s}\{e_{k+m}\{\lambda\} = g^2(\lambda) \qquad \text{(B-1.2)}$$

$$s(m,\lambda) = 0 \text{ for } m \neq 0 \qquad \text{(B-1.3)}$$

When m = 0, Equation (B-1.1) reduces to

$$\begin{aligned} E_{n,s}\{e_k e_{k+m}|\lambda\} &= E_{n,s}\{e_k^2|\lambda\} \\ &= E_{n,s}\{[c_k^2[\operatorname{sgn}(c_k + \nu_k)]^2 + b_k^2[\operatorname{sgn}(b_k + \mu_k)]^2 \\ &\quad + \nu_k^2[\operatorname{sgn}(c_k + \nu_k)]^2 + \mu_k^2[\operatorname{sgn}(b_k + \mu_k)]^2 \\ &\quad - 2c_k b_k \operatorname{sgn}(c_k + \nu_k) \operatorname{sgn}(b_k + \mu_k) \\ &\quad - 2\nu_k \mu_k \operatorname{sgn}(c_k + \nu_k) \operatorname{sgn}(b_k + \mu_k) \\ &\quad - 2c_k \mu_k \operatorname{sgn}(c_k + \nu_k) \operatorname{sgn}(b_k + \mu_k) \\ &\quad - 2b_k \nu_k \operatorname{sgn}(c_k + \nu_k) \operatorname{sgn}(b_k + \mu_k) \\ &\quad + 2c_k \nu_k[\operatorname{sgn}(c_k + \nu_k)]^2 \\ &\quad + 2b_k \mu_k[\operatorname{sgn}(b_k + \mu_k)]^2]|\lambda\} \end{aligned} \qquad \text{(B-1.4)}$$

But,

$$E_n\{\operatorname{sgn}(c + y)^2\} = 1 \qquad \text{(B-1.5)}$$

$$E_n\{y \operatorname{sgn}(c + y)^2\} = 0 \qquad \text{(B-1.6)}$$

$$E_n\{y^2 \operatorname{sgn}(c + y)^2\} = \sigma_y^2 \qquad \text{(B-1.7)}$$

$$E_n \{x \operatorname{sgn}(c + y) \operatorname{sgn}(b + x)\}$$

$$= \operatorname{erf}\left(\frac{c}{\sqrt{2}\sigma_y}\right) \sqrt{2/\pi}\, \sigma_x \exp\left(-\frac{b^2}{2\sigma_x}\right) \qquad \text{(B-1.8)}$$

$$E_n \{y \operatorname{sgn}(c + y) \operatorname{sgn}(b + y)\}$$

$$= \operatorname{erf}\left(\frac{b}{\sqrt{2}\sigma_x}\right) \sqrt{2/\pi}\, \sigma_y \exp\left(-\frac{c^2}{2\sigma_y^2}\right) \qquad \text{(B-1.9)}$$

$$E_n \{xy \operatorname{sgn}(c + y) \operatorname{sgn}(b + x)\}$$

$$= \sqrt{2/\pi}\, \sigma_y \exp\left(-\frac{c^2}{2\sigma_y^2}\right) \cdot \sqrt{2/\pi}\, \sigma_x \exp\left(-\frac{b^2}{2\sigma_x^2}\right) \qquad \text{(B-1.10)}$$

By considering first the average with respect to the noise, and using the results from Equations (B-1.5) - (B-1.10), it yields

$$E_n \{e_k^2\} = c_k^2 + b_k^2 + 2\sigma^2 - 2c_k b_k \operatorname{erf}\left(\frac{c_k}{\sqrt{2}\sigma}\right) \operatorname{erf}\left(\frac{b_k}{\sqrt{2}\sigma}\right)$$
$$- \frac{8\sigma^2}{\pi} \exp\left(-\frac{c_k^2}{2\sigma^2}\right) \exp\left(-\frac{b_k^2}{2\sigma^2}\right)$$
$$- 2c_k\sigma \sqrt{2/\pi} \operatorname{erf}\left(\frac{c_k}{\sqrt{2}\sigma}\right) \exp\left(-\frac{b_k^2}{2\sigma^2}\right)$$
$$- 2b_k\sigma \sqrt{2/\pi} \operatorname{erf}\left(\frac{b_k}{\sqrt{2}\sigma}\right) \exp\left(-\frac{c_k^2}{2\sigma^2}\right) \qquad \text{(B-1.11)}$$

It now remains to average $E_n\{e_k^2\}$ over the signal distribution. With c_k and b_k defined in (A-1.4), and substituting it in (B-1.11) and averaging over all equally likely outcomes of the symbol d_k, it results

$$\frac{E_{n,s}\{e_k^2|\lambda\}}{N_o\Delta T} = 1 + \Delta R_s + \frac{(\Delta - 2\lambda)^2 R_s}{\Delta} - 2(\Delta - 2\lambda)R_s \operatorname{erf}(\sqrt{\Delta R_s}) \cdot$$

$$\operatorname{erf}\left(\frac{(\Delta - 2\lambda)}{\sqrt{\Delta}}\sqrt{R_s}\right) - \frac{2}{\pi}\exp(-\Delta R_s)\exp\left(-\frac{(\Delta - 2\lambda)^2}{\Delta}R_s\right)$$

$$- 2\sqrt{R_s/\pi}\operatorname{erf}(\sqrt{\Delta R_s})\exp\left(-\frac{(\Delta - 2\lambda)^2}{\Delta}R_s\right)$$

$$-2\frac{(\Delta - 2\lambda)}{\sqrt{\Delta\pi}}\sqrt{R_s}\operatorname{erf}\left(\frac{(\Delta - 2\lambda)}{\sqrt{\Delta}}\sqrt{R_s}\right)\exp(-\Delta R_s)$$

$$,\lambda \leq \Delta. \qquad \text{(B-1.12)}$$

Then

$$h(\lambda) = \frac{S(0,\lambda)}{N_o\Delta T} = F\{\frac{R(0,\lambda)}{N_o\Delta T}\} = \frac{E_{n,s}\{e_k^2|\lambda\} - g^2(\lambda)}{N_o\,\Delta T} =$$

$$1 + \Delta R_s\{1 - [\operatorname{erf}(\sqrt{\Delta R_s})]^2\} + \frac{(\Delta - 2\lambda)^2}{\Delta}R_s\{1 -$$

$$[\operatorname{erf}((\Delta - 2\lambda)\sqrt{R_s/\Delta})]^2\} - \frac{1}{\pi}\{[\exp(-\Delta R_s)]^2$$

$$+ [\exp(\frac{(\Delta - 2\lambda)^2}{\Delta}R_s)]^2\} - 2\sqrt{R_s/\pi\Delta}\{\Delta\operatorname{erf}(\sqrt{\Delta R_s})$$

$$\exp(-\Delta R_s) + (\Delta - 2\lambda)\operatorname{erf}((\Delta - 2\lambda)\sqrt{R_s/\Delta})\cdot$$

$$\exp\left(-\frac{(\Delta - 2\lambda)^2}{\Delta}R_s\right)\}, \lambda \leq \Delta. \qquad \text{(B-1.13)}$$

when $\lambda = 0$

$$h(0) = 1 + 2R_s \{1 - [\mathrm{erf}\sqrt{\Delta R_s}]^2\} - \frac{2}{\pi}[\exp(-\Delta R_s)]^2$$

$$- 4\sqrt{R_s/\pi\Delta}\ \{\Delta \mathrm{erf}(\sqrt{\Delta R_s})\ \exp(-\Delta R_s)\} \qquad \text{(B-1.14)}$$

(2) Squaring Loop Type Early-Late-Gate-Integration Type of Bit Synchronizer

To evaluate $S(\omega,\lambda)$ defined by Equation (10) of the main text, the first term is given below

$$E_{n,s}\{e_k e_{k+m}|\lambda\} = E_{n,s}\{(c_k^2 + 2c_k\nu_k + \nu_k^2 - b_k^2 - 2b_k\mu_k - \mu_k^2) \cdot$$

$$(c_{k+m}^2 + 2c_{k+m}\nu_{k+m} + \nu_{k+m}^2 - b_{k+m}^2 - 2b_{k+m}\mu_{k+m} - \mu_{k+m}^2)|\lambda\} \qquad \text{(B-2.1)}$$

When $m \neq 0$, e_k and e_{k+m} are mutually statistically independent random variables. Equation (B-2.1) yields

$$E_{n,s}\{e_k e_{k+m}|\lambda\} = E_{n,s}\{e_k|\lambda\}\ \{E_{n,s}\ e_{k+m}|\lambda\} = g^2(\lambda) \qquad \text{(B-2.2)}$$

Then

$$S(\omega,\lambda) = 0 \text{ for } m \neq 0 \qquad \text{(B-2.3)}$$

When $m = 0$, Equation (B-2.1) reduces to

$$E_{n,s}\{e_k^2|\lambda\} = c_k^4 - 2c_k^2b_k^2 + b_k^4 + 4c_k^3\nu_k - 4c_k^2b_k\mu_k - 4c_kb_k^2\nu_k$$

$$+ 4b_k^3\mu_k + 4c_k^2\nu_k^2 - 8c_kb_k\nu_k\mu_k + 4b_k^2\mu_k^2 + 4c_k\nu_k^3 - 4c_k\nu_k\mu_k^2$$

$$-4b_k\nu_k^2\mu_k + 4b_k\mu_k^3 + \nu_k^4 - 2\nu_k^2\mu_k^2 + \mu_k^4 \qquad \text{(B-2.4)}$$

but

$$E_n\{c^3y\} = E_n\{b^3x\} = E_n\{c^2bx\} = E_n\{cb^2y\} = 0 \qquad \text{(B-2.5)}$$

$$E_n\{c^2y^2\} = c^2\sigma_y^2 \qquad \text{(B-2.6)}$$

$$E_n\{b^2x^2\} = b^2\sigma_y^2 \qquad \text{(B-2.7)}$$

$$E_n\{c^2yx\} = E_n\{b^2yx\} = E_n\{cbyx\} = 0 \qquad \text{(B-2.8)}$$

$$E_n\{cy^3\} = E_n\{bx^3\} = E_n\{cyx^2\} = E_n\{by^2x\} = 0 \qquad \text{(B-2.9)}$$

$$E_n\{y^2x^2\} = \sigma_y^2\sigma_x^2 \qquad \text{(B-2.10)}$$

$$E_n\{y^4\} = 3\sigma_y^4 \qquad \text{(B-2.11)}$$

$$E_n\{x^4\} = 3\sigma_x^4 \qquad \text{(B-2.12)}$$

By considering first the average with respect to the noise, and using the results from Equation (B-2.5) to Equation (B-2.12), it yields

$$E_n\{e_k^2|\lambda\} = c_k^4 - 2c_k^2b_k^2 + b_k^4 + 4c_k^2\sigma^2 + 4b_k^2\sigma^2 + 4\sigma^4 \qquad \text{(B-2.13)}$$

It now remains to average $E_n\{e_k^2\}$ over the signal distribution. With c_k and b_k defined in (A-1.4), and substituting it in Equation(B-2.13) and averaging over all equally likely outcomes of the symbol d_k, it results

$$\frac{E_{n,s}\{e_k^2|\lambda\}}{(N_o\ T)^2} = 1 + [2\Delta + \frac{2(\Delta - 2\lambda)^2}{\Delta}]R_s$$

$$+ [\Delta^2 - 2(\Delta - 2\lambda)^2 + \frac{(\Delta - \lambda)^4}{\Delta^2}]R_s^2 \qquad \text{(B-2.14)}$$

Then

$$h(\lambda) = \frac{S(0,\lambda)}{N_o\Delta T)^2} = F\ \frac{R(0,\lambda)}{(N_o\Delta T)^2} = \frac{E_{n,s}\{e_k^2|\lambda\} - g^2(\lambda)}{(N_o\Delta T)^2}$$

$$= 1 + 4\Delta R_s + 8\ \frac{\lambda^2}{\Delta}\ R_s - 8\lambda R_s, \lambda \leq \Delta. \qquad \text{(B-2.15)}$$

when $\lambda = 0$

$$h(0) = 1 + 4\Delta R_s \qquad \text{(B-2.16)}$$

APPENDIX C

Evaluation of $\int_0^\lambda g_n(y)\, dy$

$$\int_0^\lambda g_n(y)\, dy = \int_0^\lambda \frac{1}{2}\{\Delta \operatorname{erf}(\sqrt{\Delta R_s}) - (\Delta - 2y)\operatorname{erf}(\frac{(\Delta - 2y)\sqrt{R_s}}{\sqrt{\Delta}}) + \sqrt{\Delta/\pi R_s}\,[\exp(-\Delta R_s) - \exp(-\frac{(\Delta - 2y)^2 R_s}{\Delta})]\}\, dy$$

$$, \lambda \leq \Delta \qquad \text{(C-1)}$$

$$\int_0^\lambda \Delta \operatorname{erf}(\sqrt{\Delta R_s})\, dy = \Delta\lambda \operatorname{erf}(\sqrt{\Delta R_s}) \qquad \text{(C-2)}$$

$$\int_0^\lambda (\Delta - 2y)\operatorname{erf}(\frac{(\Delta - 2y)\sqrt{R_s}}{\sqrt{\Delta}})\, dy = -\frac{\Delta}{4R_s}\{[\frac{(\Delta - 2\lambda)^2 R_s}{\Delta} - \frac{1}{2}]\cdot \operatorname{erf}(\frac{(\Delta - 2\lambda)\sqrt{R_s}}{\sqrt{\Delta}}) + \frac{(\Delta - 2\lambda)\sqrt{R_s}}{\sqrt{\pi\Delta}} \exp(-\frac{(\Delta - 2\lambda)^2 R_s}{\Delta}) - (\Delta R_s - \frac{1}{2}) \operatorname{erf}(\sqrt{\Delta R_s}) - \sqrt{\Delta R_s/\pi}\, \exp(-\Delta R_s)\} \qquad \text{(C-3)}$$

Note

$$\int z \operatorname{erf} z\, dz = \frac{1}{2}[(z^2 - \frac{1}{2}) \operatorname{erf} z + \frac{z}{\sqrt{\pi}} \exp(-z^2)] + C$$

$$\int_0^\lambda \sqrt{\Delta/\pi R_s}\, \exp(-\Delta R_s)\, dy = \sqrt{\Delta\lambda^2/\pi R_s}\, \exp(-\Delta R_s) \qquad \text{(C-4)}$$

$$\int_0^{\lambda} \sqrt{\Delta/\pi R_s}\ \exp\left(-\frac{(\Delta - 2y)^2 R_s}{\Delta}\right) dy = -\frac{\Delta}{4R_s} \cdot \left[\operatorname{erf}\left(\frac{(\Delta - 2\lambda)\sqrt{R_s}}{\sqrt{\Delta}}\right) - \operatorname{erf}(\sqrt{\Delta R_s})\right] \qquad \text{(C-5)}$$

Combining (C-2), (C-3), (C-4), and (C-5) and simplfying

$$\int_0^{\lambda} g_n(y)\ dy = \frac{1}{2}\left\{\left[\Delta\lambda - \frac{\Delta}{8R_s} - \frac{\Delta^2}{4}\right]\operatorname{erf}(\sqrt{\Delta R_s}) + \left[\frac{\Delta}{8R_s} + \frac{(\Delta - 2\lambda)^2}{4}\right] \cdot \operatorname{erf}\left(\frac{(\Delta - 2\lambda)\sqrt{R_s}}{\sqrt{\Delta}}\right) + \left(\sqrt{\Delta\lambda^2/\pi R_s} - \frac{1}{4}\sqrt{\Delta^3/\pi R_s}\right) \exp(-\Delta R_s) + \frac{\sqrt{\Delta}(\Delta - 2\lambda)}{4\sqrt{\pi R_s}} \exp\left(-\frac{(\Delta - 2\lambda)^2 R_s}{\Delta}\right)\right\}, \quad \lambda \leq \Delta. \qquad \text{(C-5)}$$

Note, as $R_s \to \infty$

$$\int_0^{\lambda} g_n(y)\ dy \to \frac{\lambda^2}{2}, \quad \lambda \leq \Delta. \qquad \text{(C-6)}$$

APPENDIX D

Evaluation of σ_λ^2 for Large Value $R_s\zeta_s$

First evaluating C_1, from Equation (29) and Equation (39) of the main text

$$\int_{-\Delta}^{\Delta} C_1 \exp\left(-\frac{2R_s\zeta_s}{\Delta}\lambda^2\right) d\lambda =$$

$$C_1 \sqrt{\Delta\pi/2R_s\zeta_s}\ \mathrm{erf}\left(\sqrt{2\Delta R_s\zeta_s}\right) = 1 \qquad \text{(D-1)}$$

$$C_1 = \frac{1}{\sqrt{\Delta\pi/2R_s\sigma_s}\ \mathrm{erf}\left(\sqrt{2\Delta R_s\zeta_s}\right)} \qquad \text{(D-2)}$$

Then from Equation (36) of the main text

$$\sigma_\lambda^2 = C_1 \int_{-\Delta}^{\Delta} \lambda^2 \exp\left(-\frac{2R_s\zeta_s}{\Delta}\lambda^2\right) d\lambda$$

$$= C_1 \int_{-\sqrt{2\Delta R_s\zeta_s}}^{\sqrt{2\Delta R_s\zeta_s}} \left(\frac{\Delta}{2R_s\zeta_s}\right)^{3/2}\lambda^2 \exp(-\lambda^2)\, d\lambda$$

$$= C_1\left(\frac{1}{2R_s\zeta_s}\right)^{3/2}\left[-\sqrt{2\Delta R_s\zeta_s}\exp(-2\Delta R_s\zeta_s)\right.$$

$$\left. + \frac{\sqrt{\pi}}{2}\mathrm{erf}\left(\sqrt{2\Delta R_s\zeta_s}\right)\right] \qquad \text{(D-3)}$$

when $R_s\zeta_s \to \infty$

$$\sigma_\lambda^2 = \frac{\Delta}{4R_s\zeta_s} \qquad \text{(D-4)}$$